Fall 12-31-2023

Borophene and Graphene for Non-Enzymatic Biosensor- ab-initio study

Omar A. Ismail
American University in Cairo, omar_a_ismail@aucegypt.edu

The American University in Cairo

الجامعة الأمريكية بالقاهرة

Graduate Studies

Borophene and Graphene for Non-Enzymatic Biosensor- ab-initio study

A THESIS SUBMITTED BY

Omar Ahmed Mohamed Ismail

TO THE

The Mechanical Engineering Department

14th of June 2023

in partial fulfillment of the requirements for the degree of
Masters of Science in Mechanical Engineering

Declaration of Authorship

I, Omar Ahmed Mohamed Ismail, declare that this thesis titled, “Borophene and Graphene for Non-enzymatic Biosensor- *ab-intio* study” and the work presented in it are my own. I confirm that:

- This work was done wholly or mainly while in candidature for a research degree at this University.
- Where any part of this thesis has previously been submitted for a degree or any other qualification at this University or any other institution, this has been clearly stated.
- Where I have consulted the published work of others, this is always clearly attributed.

- Where I have quoted from the work of others, the source is always given. With the exception of such quotations, this thesis is entirely my own work.
- I have acknowledged all main sources of help.
- Where the thesis is based on work done by myself jointly with others, I have made clearexactly what was done by others and what I have contributed myself.

Signed:

Omar Ahmed Mohamed Ismail

_____

Date:

16/06/2023

_____

Abstract

Non-enzymatic glucose sensing holds promise to overcome limitations associated with glucose oxidase, such as oxygen dependence and short shelf life. This study explores the potential sensing capabilities of borophene and graphene through direct interaction with various compounds, including β-glucose, uric acid, ascorbic acid, fructose, and acetaminophen. Using Density Functional Theory (DFT), we calculated binding energies and the respective Density of States (DOS) for these adsorbates on both graphene and borophene surfaces. Preliminary results suggest that borophene might exhibit nearly twice the affinity for β-glucose compared to graphene. Moreover, the calculated Density of States reveals distinct distortions in the electronic states of both graphene and borophene upon β-glucose adsorption. These results suggest unique electronic responses of these two-dimensional materials to glucose adsorption. However, further detailed studies and calculations are crucial for more comprehensive conclusions.

Acknowledgements

I thank God, who has given me the means to continue my study and the fortitude to persevere through obstacles. I'd like also to thank my loved ones, especially my parents, who have been there for me through thick and thin as I pursued my education. My inspiration and drive come from their unending support, encouragement, and sacrifices (Thank you Mum and Dad). In addition, I'd want to express my deepest gratitude to Prof. Mohamed Serry and Dr. Karim Elgammal for providing me with invaluable feedback, suggestions, and encouragement during the process of writing my thesis. Having access to their knowledge, feedback, and support has been crucial to finishing this thesis. Special thanks to Mohamed Waheed Tawfik, who didn't just suggest this project, but also this project wouldn't have been completed and Ahmed Ali for the huge encouragement.

Last but not least, my classmates and friends have been invaluable travelling companions, providing me with invaluable support and encouragement. Finally, I would also like to express my appreciation to everyone on the professors and staff of the School of Sciences and Engineering at the American University in Cairo for their contributions to my education and development.

Contents

List of Figures

List of Abbreviations

WHO	**World Health Organization**
CDC	**Center for Disease Control and Prevention**
CGM	**Continuous glucose monitoring**
E	**Energy in eV**
QE	**Quantum Espresso**
CNTs	**Carbon nanotubes**
MWCNTs	**Multi-walled carbon nanotubes**
SCF	**Self-Consistent Calculations**
SPC	**Single Point Calculations**
NSCF	**Non-Self-Consistent Calculations**
PAW	**Projected Augmented Wave**
GBRV	**Garrity, Bennett, Rabe, and Vanderbilt**
DOS	**Density of States**

List of Symbols

$E_{binding}$	Binding energy in eV
$E_{analyte}$	Analyte energy in eV
E_{total}	System total energy in eV

Chapter 1

Introduction

- Diabetes

Diabetes affects millions globally. According to the CDC, 415 million people have diabetes, and by 2040, that figure will approach half a billion[1]. High blood sugar (glucose) is caused by the body not producing enough insulin or not using it effectively. Type 1 diabetes is diagnosed in childhood or adolescence when the immune system attacks insulin-producing cells, while type 2 diabetes is more common in adults and caused by hereditary and lifestyle factors[2]. Type 1 diabetes affects 10% of diabetics, usually children and teens. The immune system mistakenly attacks insulin-producing pancreatic cells, causing this illness. Insulin injections or pumps are required to manage type 1 diabetes. 90% of diabetics have type 2. Obesity, inactivity, and poor diets cause the condition. Although diet and exercise can control type 2 diabetes, some people may need medication[3].

Diabetes can change lives. High blood sugar damages blood vessels and neurons throughout the body, causing several health issues. Nephropathy, retinopathy, and cardiovascular disease can cause renal failure, blindness, and heart attacks[3]. Untreated diabetic foot sores and infections can lead to amputation[3]. Diabetes makes injury and disease recovery harder. These negatives can lower a person's level of living or kill them. In 2019, the WHO reported that diabetes caused 1.5 million deaths, making it the tenth greatest cause of death [3].

Medication, lifestyle changes, and self-care help manage diabetes. Diabetes can be managed to prevent problems. Diabetes patients should also follow a healthy lifestyle. Examples include eating a low-sugar, low-saturated-fat diet, exercising, and quitting smoking. Diabetics must monitor their glucose, blood pressure, and cholesterol in addition to food and exercise. Cardiovascular disease prevention requires ongoing monitoring.

Despite illness management challenges, diabetics can live full and active lives. Therapy and self-care help many diabetics control their blood sugar and avoid complications. However, diabetics should work with their doctors to build a personalized treatment plan that addresses their symptoms, goals, and condition. Diabetics can improve their health by working together to make healthier choices.

Pancreas transplantation can now permanently treat type 1 diabetes [4], [5]. A donor pancreas replaces a patient's damaged pancreatic in this surgery. The surgery is designated for type 1 diabetics with serious problems such kidney or nerve injury that cannot be controlled with other procedures. A simultaneous

pancreas-kidney transplant (SPK) is possible [4], [5]. The donor pancreas is surgically linked to the recipient's blood vessels and digestive system to create insulin and manage blood sugar.

Pancreas transplantation for type 1 diabetics is risky but life-changing. Blood loss, infection, and anaesthesia issues are dangers of every major surgery. Immunosuppressive medicines used to prevent the body from rejecting the donor pancreas increase the risk of infections and other problems. Despite these dangers, pancreas transplantation can be a viable treatment for type 1 diabetics with severe problems who cannot manage their illness.

- Sensors

Biosensors measure biological signals such blood glucose[6], [7]. They offer a non-invasive, cost-effective way to monitor a number of ailments, making them increasingly important in healthcare. Biosensors typically have an enzyme or antibody and a transducer that turns the biological signal into an electrical or visual signal. Recent biosensor advances include real-time glucose-monitoring biosensors that can be worn.

Biosensors can help manage diabetes. Diabetics must check their blood sugar levels to avoid neurological, kidney, and cardiovascular issues. Fingerstick blood glucose monitoring is uncomfortable and inconvenient, resulting in low compliance. Biosensors allow diabetics to monitor glucose levels continuously and non-invasively.

Biosensor technology for diabetes control has advanced greatly. One such breakthrough is continuous glucose monitoring (CGM) systems, which use a tiny sensor implanted under the skin to measure interstitial fluid glucose levels[6], [7]. A receiver displays real-time glucose measurements from the sensor. Diabetics can constantly monitor and alter their glucose levels. Non-invasive biosensors using optical detection and spectroscopy to measure glucose levels without a blood sample are being developed alongside CGM.

Closed-loop systems, often known as artificial pancreas systems, are developing biosensors for diabetes management[8]. These CGM-insulin systems automatically adjust insulin delivery based on glucose levels. These technologies make diabetes management simpler by eliminating the need to manually check glucose levels and adjust therapy.

As a non-invasive, continuous glucose monitoring tool, biosensors are vital for diabetes care. Biosensor technology has led to wearable biosensors, continuous glucose monitoring devices, and closed-loop systems. These advances will make managing diabetes easier and help diabetics avoid problems. As biosensor technology advances, new diabetes care methods may emerge.

Chapter 2

Literature Review

Diabetes is a global epidemic. Insulin deficiency or insulin resistance induce the disorder [2]. In 2019, the WHO reported that diabetes killed 1.5 million people and affected 463 million[3]. It causes blindness, kidney failure, amputations, and heart attacks[3]. Diabetics must eat well and exercise while monitoring their glucose levels. Thus, ongoing monitoring requires non-invasive testing.

The urgent requirement for glucose detection has pushed scientific frontiers in various domains. M. H. Hassan et al. reported in 2021 that glucose sensor research increased from 800 articles in 2011 to over 1800 in 2020 [9]. Blood, sweat, interstitial fluids, tears, saliva, and urine can be used to classify glucose sensors[10]. Oliver et al. introduced a more detailed classification by staggering the sensors first if they are one-time samples or continuous, then dividing each with the most used continuous sampling techniques, whether invasive or non-invasive, and their associated technologies [11].

- ### Types of Glucose Sensors

Point sample failed to meet the growing demand for accurate and consistent measurements from diabetics. Finger-prick glucometers hurt[12]. Urine Dipsticks also track glucose poorly [13]. Continuous techniques for painless monitoring are prioritized [9][12][14]. Transdermal, optical, and electrochemical are non-invasive. Transdermal technologies use physical energy to extract glucose from interstitial fluids or blood, including impedance spectroscopy[15], sonophoretic[16], skin suction blister [17][18], reverse iontophoresis [19]. However, optical glucose sensors depend on lighting, light scattering, and refraction, the foundations of fluorescence, surface Plasmon resonance sensors, and absorptiometry biosensors [20][21][22][23][24][25]. The optical and transdermal sensors are low-cost and non-electrical, but the optical sensors are affected by light and can only be used in a certain glucose concentration range [26][27].

The preceding methods are complex, expensive, and challenging [11]. Electrochemical sensors can test glucose levels non-invasively. Tian et al. classified electrochemical sensors by sensing material (metals, metal compounds, composites, and carbon micro or nano material) [14], while Rahman et al. classified glucose biosensors by operating principle (potentiometric, amperometric, and impedimetric (conductometric) [28]. Potentiometric sensors measure glucose concentration by measuring voltage between two electrodes at zero current. Amperometric sensors use a constant potential to adjust the output electric current with solution concentration, while impedimetric (conductometric) sensors detect concertation by changing the sensing device's conductance [14],[28]. Enzymatic and non-enzymatic electrochemical biosensors have been widely employed recently [9][10][11],[14].

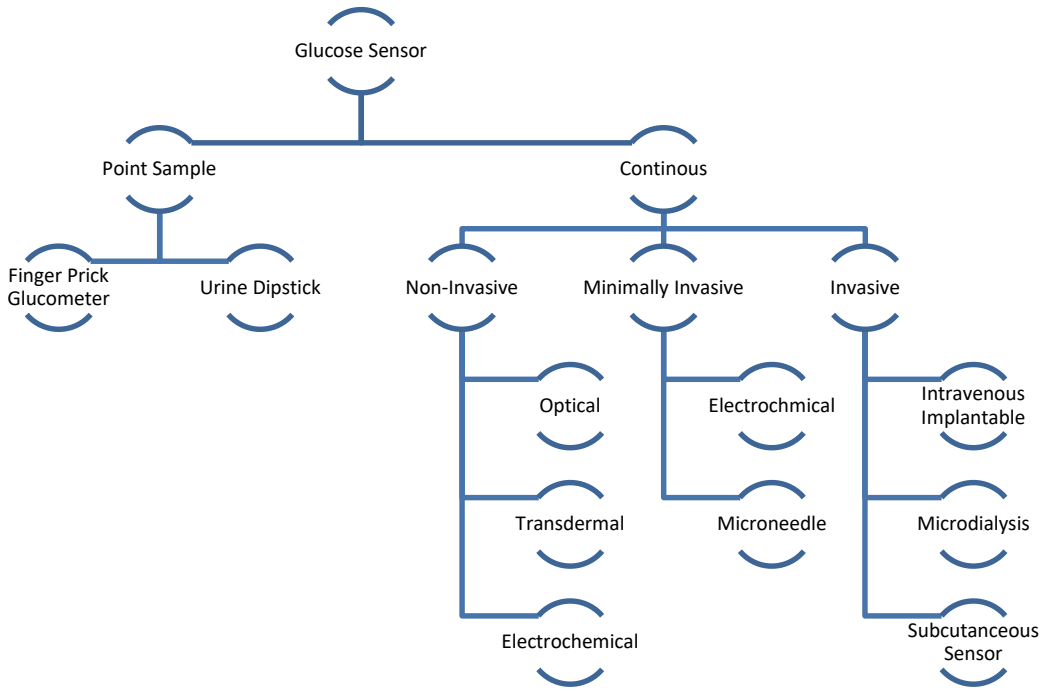

Figure 1:Different types of glucose sensor based on their measuring technique, introduced by Oliver et al. [11]

- Enzymatic Sensors

Enzymatic glucose sensors use enzymes to measure glucose. Glucose oxidase (GOx) converts glucose into hydrogen peroxide and gluconic acid. Clark and Lyon introduced it [29]. Despite sensing and detecting glucose levels, the enzyme was impacted by blood oxygen. To fix this, Updike and Hicks inserted an oxygen electrode (counter electrode) to the glucose sensor[30]. Glucose oxidase, reference, and counter electrodes make up the enzymatic glucose sensor [9].

Hydrogen peroxide and a second enzyme generate an electric signal [9]. The second enzyme's Flavin group transfers electrons to catalyze the process and provide a signal [31]. Enzymatic glucose sensors need the Flavin group to transport electrons and generate a signal. The enzymatic reaction and this glucose sensor's accuracy depend on the Flavin group. The electrical signal produced by hydrogen peroxide and peroxidase reaction is proportional to glucose content [31]. A meter or smartphone app displays the sample's glucose concentration after receiving the signal [9].

Three generations of enzymatic glucose sensors improve performance. Glucose measurement and sensor materials distinguish first-, second-, and third-generation enzymatic glucose sensors [9]. Enzymatic glucose sensors initially contained solely glucose oxidase. Second-generation enzymatic glucose sensors enhanced glucose and glucose oxidase signals with peroxidase. Amplification improved detection, precision, and sample contamination. Nanomaterials and polymers improved third-generation enzymatic glucose sensors. These compounds removed mediators [11].

1. First Generation Enzymatic sensor

As seen in Figure 2, glucose oxidase regenerates the Flavin group when glucose is converted to gluconic acid. Yanan Zhang et al. employed Nafion membrane with varied porosities to eliminate the effect of acetaminophen on glucose measurement [32]. By inhibiting acetaminophen diffusivity in the membrane, their sensor increased glucose blood sensitivity and response time. Malitesta et al. developed a glucose oxidase sensor utilizing a 10nm poly(ophenylenediamine) (PPD) film [33]. The sensor responded in 1s and detected 14.2 mM with a current density of 181µA/cm2 and an electrode voltage difference of 0.65V.

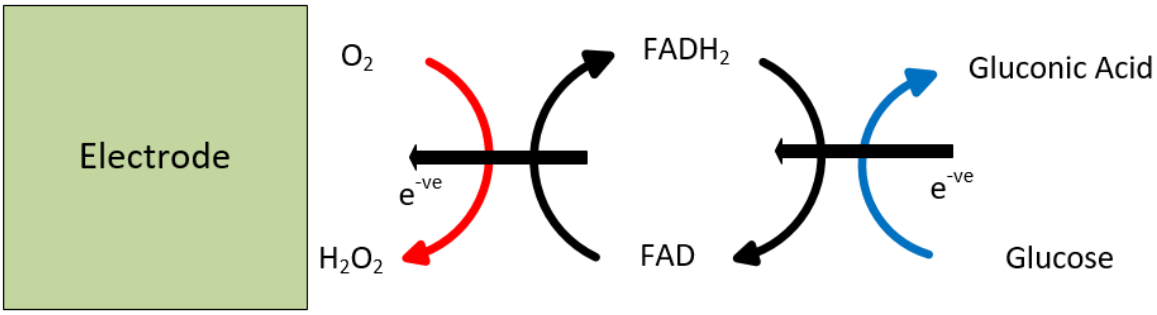

Figure 2: A schematic of First Generation sensor electrochemical cycle and sensing mechanism

Sasso et al. built a glucose sensor on a platinized, reticulated vitreous carbon (RVC) electrode using a 1,2-dlamlnobenzene-polymerized electrode [34]. The polymer coating thermally stabilized glucose oxidase, extending shelf life to 1.5 months. It also lowered the sensor's sensitivity to uric acid, ascorbic acid, and other blood enzymes and acids, preventing inaccurate glucose measurements [34]. Kafi et al. proposed immobilizing glucose oxidase (GOD) using multiporous nanofibers (MPNFs) of SnO2 on a Prussian blue (PB)-modified gold (Au) electrode containing chitosan to make an enzyme electrode [35]. With a detection limit of 0.05mM, glucose concentration was linear between 0.5 and 5mM.

R. Alhans et al. evaluated glucose sensing enhancement on gold printed circuit boards with single and multi-walled carbon nanotubes (CNTs) [36]. Single-walled CNTs had a sensing range of 1mM-100mM and a detection limit of 0.1mM in 5s reaction time. Baek et al. [37] and Mei [38] suggested employing Cu-nanoflower decorated gold nanoparticles-graphene oxide nanofiber and Ni/CoO carbon nanofiber sequentially to improve sensor sensitivity and selectivity. The Cu-nanoflower detected glucose in a range of 0.001–0.1 mM with a detection limit of 0.018 µM, whereas the Ni/CoO nanofiber had an excellent linear range from 0.25 µM to 600 µM and an exceedingly low detection limit of 0.03 µM [37], [38].Nanomaterials reduced glucose sensor detection range and limit.

Due of its affordability, the first-generation non-enzymatic sensor was imprecise and prone to interference. Oxygen variation and deficiency produce these interferences [9]. Second-generation glucose sensors were developed to reduce oxygen dependence.

2. Second Generation Enzymatic sensor

In order to further improve the glucose sensor precision and sensitivity and cancel the reliance on glucose oxidase, second generation sensors used an artificial mediator to help the Flavin group in electron transportation on the electrode surface as illustrated in Figure 3. These artificial mediators are made from organic salts including ferrocene, quinone compounds, transition-metal complexes, etc… [39]–[41].

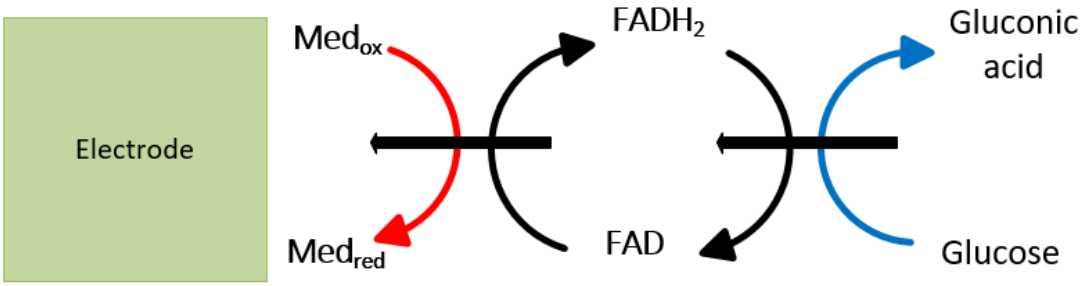

Figure 3: A schematic of Second Generation sensor electrochemical cycle and sensing mechanism

Marquitan et al. tried modify the polymer enzyme coating by using poly(4-styrene sulfonate-co-glycidyl methacrylate-co-butyl acrylate) as a redox mediator in his miniature glucose sensor[8]. In order to fabricate it, the process was held on two complex steps involving activating cross linkers, and electro deposition. This new polymer/enzyme helped in detecting glucose concentrations up to 15mM. In addition, the new polymer/enzyme was immune to ascorbic acid and uric acid influence[8]. T. Bobrowski et al. constructed an enzymatic glucose sensor that can be implanted in the pancreas and provide continuous readings[8]. Their sensor operated up to 180 days, but implantable sensors should have longer lifetime since the patient is required to pass through a painful and expensive procedure.

It is apparent that carbon nanotubes (CNTs) has a great influence on enhancing glucose biosensors. Gallay et al. used multi-walled carbon nanotubes (MWCNTs) to construct a highly sensitive glucose biosensor [42]. The utilization of MWCNTs enhanced the contact of the enzymatic biotinylated horseradish peroxidase with the electrode, hence enhancing the overall electron exchange reaching a sensitivity of 4.8 $\mu.A.mM^{-1}$ in a linear range of 50-500µM

The second generation of sensors has proven to improve precision and sensitivity, yet it still has a very low lifetime. Besides, there are multiple difficulties in the manufacturing process since the artificial mediator should always be in good adhesion and contact with the electrode to increase the electron transfer efficiency[9].

3. Third Generation Enzymatic sensor

Since the last two generations had either an oxygen or artificial redox as a mediator between the Flavin group and the electrode, this led to several problems in the electron-exchange and sensitivity of the electrode[9]. The Third generation enzymatic glucose sensor remove the mediator making the flavin group responsible for the oxidation of the glucose to gluconic acid and transferring the electrons directly to the electrode.

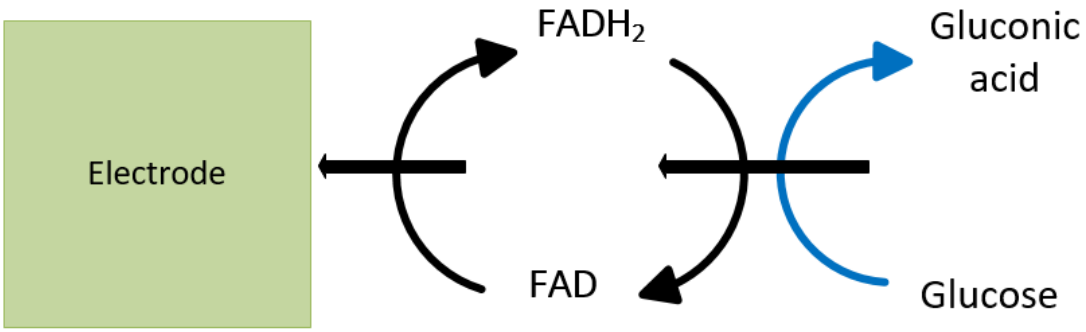

Figure 4: A schematic of Third Generation sensor electrochemical cycle and sensing mechanism

whereas the third generation of sensors utilizes improved materials for increased durability. As technology advances, enzymatic glucose sensors could improve. Willner et al investigated how to increase the electron-exchange between the Flavin group and the electrode[43]. They used pyrroloquinoline quinone with the ferrocene modified FAD on a gold electrode. This enzyme led to an improvement in the electronic properties of the flavin group and the direct electron-exchange with the electrode itself. Another study presented by Zayats et al. reviewed the different enzymes for electronic improvement whether flavin adenine dinucleotide (FAD)-containing enzymes (flavoenzymes) or pyrroloquinoline quinone (PQQ)[44]. They also highlighted the effect of using carbon nanotubes and gold nanoparticles for further enhancements in electron transport from the redox center to the electrode.

Polymeric 3-Aminophenyl Boronic Acid Monolayer was also introduced as a good candidate for reconstituting the Flavin group in the biosensor[45]. It was found that the glucose sensor had a concentration range of 1-17mM and a response time of 12s and a sensitivity of 5 µA/mM. Tasviri et al. proposed using nano-composite material with an amino radical as an enzyme and to enhance the

electronic property carbon nanotubes were also added[46]. This enzyme resulted in a rapid response time and a linear yet narrow concentration ranges of 1.8-266µM.

Despite the high sensitivity, low cost and simplicity of enzymatic sensors, it has several limitations including their short life span [47] and deviation in readings due to environmental factors including humidity, pH level, temperature [48]–[50]and the sensor layer thickness [28], [51]. On the other hand, Non-enzymatic glucose sensors don't rely on a mediator since it mainly depends on the direct oxidation or reduction of the glucose. These sensors are known for their long life span, the ability to be reused and simplicity.

- Non-enzymatic Sensors

Since the enzymatic sensor is not eligible for continuous glucose measurements due to short life span, non-enzymatic sensors provide a solution for this drawback. However, They suffer from some drawbacks such as their low sensitivity and selectivity compared to enzymatic sensors and relatively high cost[47]. That is why there have been many contributions in order to enhance the sensitivity and selectivity of non-enzymatic sensor. One of these techniques is using metals with good electronic properties including platinum (Pt)[52]–[56], Copper (Cu)[57], [58], Nickel (Ni)[59], [60], gold (Au) [61]–[63]and silver (Ag) or their alloys including (Pt-Ag, Pt-Ni, Pt-Pb and Au-Pt) since a binding site is produced from the presence of the different atom in the structure[64]–[68].

Although the metals used in non-ezymatic glucose sensor have increased its sensitivity, some of them like platinum(Pt), gold (Au) and silver (Ag) are very expensive and rare[9]. Despite that copper is not expensive, it doesn't work efficiently in low or neutral pH and gets negatively affected by the ethanol interference[9]. Another emerging material is to use graphene and graphite due to their relatively good electronic properties, chemical stability and can immensely increase the area of interaction with glucose molecules due to its high surface-volume ratio[51]. Despite its competitive advantages that help in fabricating highly sensitive glucose sensors, they have lower detection limit compared to conventional sensors[51]. To improve its detection limit and further enhance its affinity for glucose, various researchers have tried to enhance these properties by doping the above metals including Pt, Au and Ag[9][14], [28], [51], [69]. However, it is very expensive to test for all the materials and compare between them. That is why scientists have used Density Functional Theory (DFT) and Molecular Dynamics (MD) to investigate the effect of doping, pretension, adding highly conductive substrates or defects before doing expensive experiments[70].

1. Nano-Modeling for Non-Enzymatic Sensors

Density Functional Theory (DFT) has been used to estimate graphene sensor affinity and detection limit before sensor manufacturing. Sakr et al. studied graphene as a glucose sensor experimentally and

numerically[71]. They examined glucose binding energy directly on the platinum substrate, on the pristine graphene sheet solely, and on the graphene plus platinum substrate below it. Using graphene sheet on a platinum substrate yielded the shortest glucose spacing of 3.5Å compared to 3.63Å on the platinum substrate alone [71]. Caglar et al. examined glucose adsorption on platinum-gold-doped graphene [70]. They found that gold-doped graphene had a binding energy of -0.71eV and a spacing of 2.28Å, while platinum-doped graphene had -0.38 eV and 2.39 Å. The same authors also evaluated glucose adsorption between graphene dopped with palladium (Pd) alone and graphene dopped with Pd on pyridinic nitrogen. Palladium-doped graphene and pyridinic nitrogen-doped graphene with modified palladium had glucose adsorption of -0.44 eV and -0.64 eV, respectively, with spacings of 2.49Å and 2.20Å.

Puspamitra Panigrahi et al. used DFT to investigate glucose selectivity on two-dimensional nitrogenated holey graphene (C2N) monolayer [72]. Gaseous and aqueous adsorption of glucose, fructose, and xylose. Aqueous medium improved molecule binding energies. Glucose, fructose, and xylose had binding energies of -0.93 eV, -0.84 eV, and -0.81 eV in gaseous media and -1.31, -1.23, and -1.3eV in aqueous medium. C2N demonstrated glucose selectivity in gaseous medium despite lesser sensitivity than in aqueous medium. Düzenli et al. doped Au, Cu, Ni, Pd, Pt, and Zn atoms on pyridinic nitrogen-doped graphene to evaluate glucose binding and adsorption energy in basic solution [73]. The glucose and palladium had the highest binding energy at -0.65eV, followed by copper at -0.49eV and nickel and gold at -0.3eV. They also found that water reduces the interaction of glucose on the sensor base, with glucose binding energies reaching only -0.3eV with the palladium in the basic solution compared to -0.64eV in the solution-free system [73].

Finally, borophene, a 2D conductive substance, has been discovered. Borophene, a Boron-based 2D material, has been successfully produced and is promising for non-enzymatic biosensors[74]. Cihat Tasaltin made a glucose sensor from 2D borophene in a β-rhombohedral [75] and β12 structure [76]. The borophene β12 structure on a PANI-base sensor could detect a concentration of 1 to 12 mM with a sensitivity of 96.93 µA mM-1 cm-2 and a detection limit of 0.5 mM[76]. Cihat also compared this sensor to G-PANI, TiO2/PANI-GO, and other sensors. The concentration range, limit of detection, and sensitivity were 0.02mM to 6mM, 18 µM, and 6.31 µA mM-1 cm-2 for TiO2/PANI-GO and 0.01mM to 1.48mM, 2.768 µM, and 22.1 µM for G-PANI. Unlike graphene, 2D borophene can be used as a glucose sensor [76].

There have been many studies looking for a highly selective and sensitive material for non-enzymatic glucose sensors, but few have tested the compatibility of borophene and its affinity for glucose using DFT and Molecular Dynamics.

That's why this article tests glucose's sensitivity and selectivity on graphene and borophene, the two most promising base materials for the enzymatic glucose sensor. Calculate the ground state electrical characteristics, binding energies, and density of states between glucose and the sensor material and compare it to acetaminophen (paracetamol), uric acid, ascorbic acid, and fructose. In addition, the effect of platinum substrate, the most often used, on the sensitivity of the two pure materials is examined to see if it improves or degrades a non-enzymatic glucose sensor.

Chapter 3

Methodology

In order to model the system and test the selectivity of the pristine material several steps have been performed as shown in Figure 5. First, we are trying to evaluate for a potential pristine material for non-enzymatic glucose sensor, so different molecules should be chosen to test for selectivity. In parallel, the supercell of both the graphene and borophene is constructed and relaxed using Quantum Espresso[57]–[59]. Second, the chosen molecules have been relaxed using xTB tight binding [77][78]. After that, the Adsorption Locator module in Materials Studio is utilized to orient the molecule on the surface of the pristine material [79]. Then, the molecules have been allowed to relax on the fixed pristine material to further enhance the orientation of the molecule and then the entire system's energy is calculated using Quantum Espresso[57]–[59]. In order to calculate the Density of States (DOS) and Fermi energy an additional self-consistent and Non-self-consistent calculations were done. Finally, a platinum substrate, since it is the most commonly used, is introduced to the system to test for the variation of sensitivity of the pristine material towards glucose. This DFT model calculations were done using Quantum Espresso [80]–[82] on two steps first a relaxation of the system to determine the changes in the lattice parameters and atomic positions then a Single point calculations (SPC) to calculate the final energies.

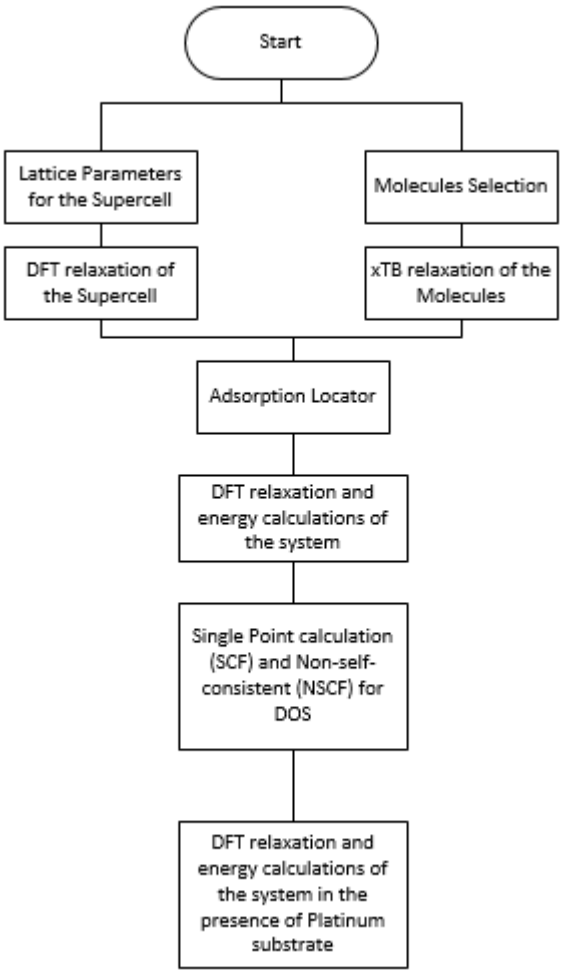

Figure 5: Steps for simulating the system

Lattice Parameters for the Supercell

The supercell had to be big enough to ensure cancelling the effect of the periodicity so the molecules will not interact with each other or other layers of pristine materials. That is why the vacuum space was initially 20 Å and a the supercell needed to be large enough to avoid any molecule to molecule interaction due to periodicity. In addition, the two pristine materials should have had an equal number of atoms of around 200 atoms. As illustrated in Figure 6 the dimensions of the borophene as stated by Zhou et al. [83] and Wang et al. [84]. As for the graphene, the supercell has been built from the modules available on Materials studio[85].

Table 1: The Final cell parameters of graphene and borophene after relaxation

	Graphene	Borophene
a (Å)	24.7640	28.6428
b (Å)	24.7640	16.3559
c (Å)	18.6227	13.4610
α	90.0000^0	90.0002^0
β	90.0000^0	89.9990^0
δ	120.0009^0	89.8402^0

The final lattice parameters after the relaxation are shown in Table 1. It can be highlighted that the lattice parameters have had some changes after the relaxation calculations. Despite this reduction, the vacuum space can be enough to eliminate the effect of periodicity in DFT calculations.

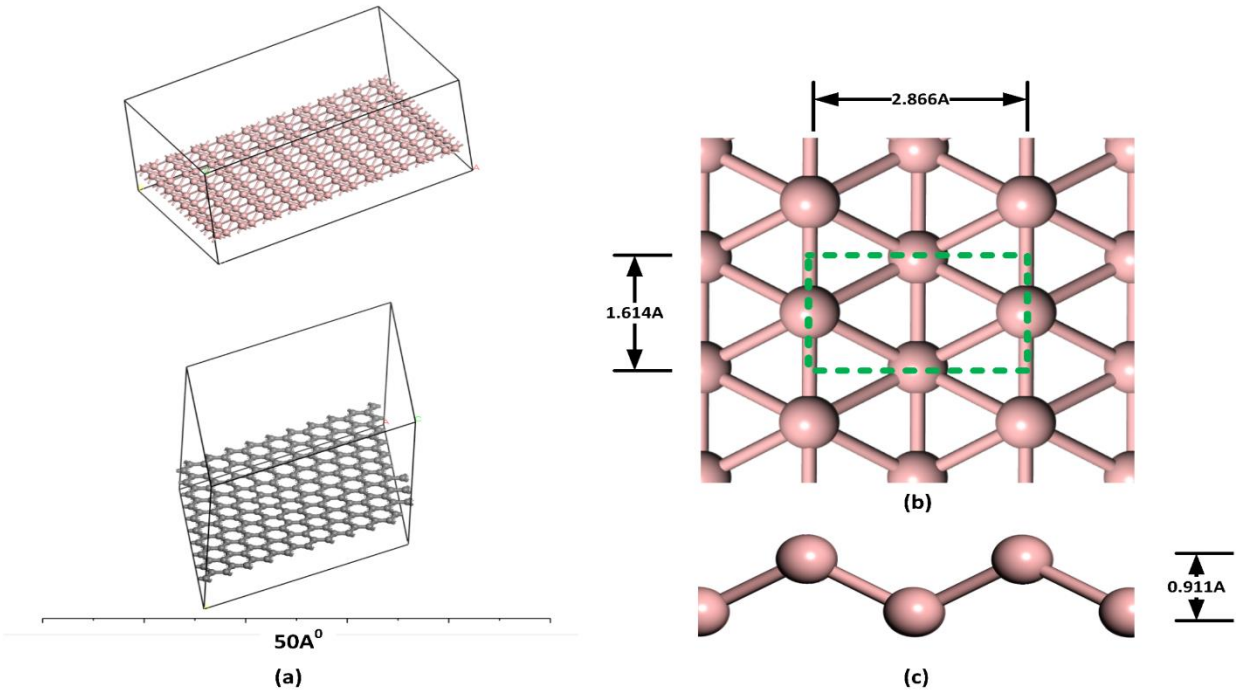

Figure 6: (a) on top is the supercell of Borophene and below it the supercell of Graphene. The Borophene structure dimensions are presented in (b) the top view, (c) the side view [83][84]

Molecule selections

In order to compare the selectivity of the two pristine material (graphene and borophene), organic and inorganic molecules that contain similar structure for glucose ($C_6H_{12}O_6$) or have been reported to alter the glucose sensor readings. It has been reported in literature that fructose ($C_6H_{12}O_6$) since it has a similar chemical composition [72], acetaminophen ($C_8H_9NO_2$) (also known as paracetamol)[86], uric acid ($C_5H_4N_4O_3$) and ascorbic acid ($C_6H_8O_6$)[87] also have influence in glucose measurement. Besides, glucose has two main forms whether alpha or beta glucose, the beta glucose was used in our simulations since it is more stable and more present in blood [72]. The molecules are shown in Figure 7.

Tight Binding Relaxation

In order to relax the molecules and at the same time manage the computational consumption, semiempirical Tight Binding xTB software is used[77][78]. The molecules were optimized using the semiempirical quantum mechanical method GFN2-xTB[88] with an energy and gradient convergence thresholds of $1x10^{-6}$ Eh ($3\ x10^{-4}$ eV) and $8x10^{-4}$ Eh/α with no lattice or periodicity.

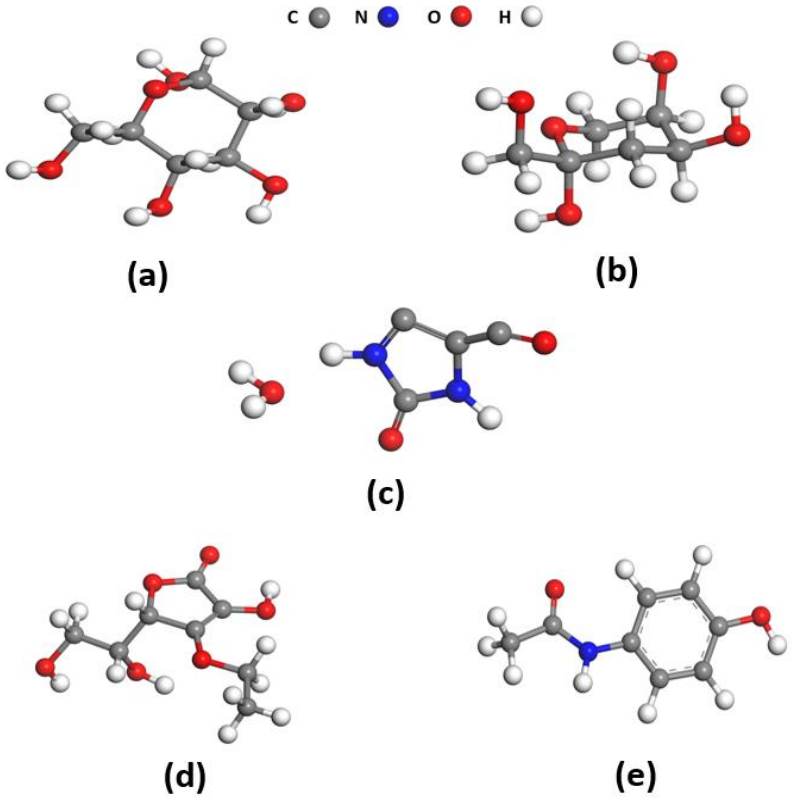

Figure 7: The adsorbates after relaxation using xTB where (a) β-glucose (b) Fructose (c) Uric Acid (d) Ascorbic Acid (e) Acetaminophen or Paracetamol

Adsorption Locator

In order to know the position and orientation of the molecule that can give the least energy either Molecular Dynamics DFT calculations in Quantum Espresso should be used or Adsorption Locator tool which rely on semi empirical kinetic energy Monte Carlo simulations introduced by Materials Studio[79]. The Molecular Dynamics DFT calculations are computationally expensive and takes a lot of time. On the other hand, Adsorption locator takes minutes to figure out the adsorbate orientation on a substrate using Monte Carlo searches. The adsorbate is rigid during the simulation, i.e. it has a fixed bond length and valence angles, this allows the molecule to rotate around it center of mass. The minimum electrostatic energy is calculated using Ewald & Group summation methods where the Forcefield was selected as Universal with a cut off adsorption distance of 7 Å. Since the adsorption locator doesn't solve using DFT, the final system energy was calculated using CASTEP module in Materials Studio.

Validity of Adsorption locator

To ensure the accuracy of the Adsorption Locator module in correctly predicting the orientation and position of the molecules on the pristine material, the First-principles relaxation calculations are carried out using Quantum Espresso[80]–[82]. The output molecule orientation from the Adsorption Locator is allowed to relax on the fixed pristine in the DFT calculations. If the molecule made an obvious change whether in its orientation or its distance from the pristine material, the Adsorption locator then fails to predict the adsorbate position with respect to the pristine material. The system was calculated with a wave function cutoff of 60Ry and charge density cutoff of 480Ry.Futhermore, the pristine material occupation was fixed, while the molecule was left to move freely in all directions. Moreover, a Gaussian smearing was used along with Grimme-D3 for van der Waals, a saw-like electric field potential and ionic dipole corrections. Energy convergence threshold of 10^{-5} and the pseudopotentials of the atoms were extracted from the Standard solid-state pseudopotentials (SSSP) available on Materials Cloud [89] [90] [91].

DFT Relaxation and SPC calculations of the system

Once the molecule position and orientation is determined using the Adsorption Locator, first-principle calculations single point calculations are preformed to calculate the binding energy of the molecules on the pristine materials on two steps. First, a geometry optimization calculations done using CASTEP module in Materials Studio where the molecules are allowed to move freely while the pristine material is fixed[92]. The exchange-correlation functional was GGA PBE and DFT-D correction is performed due to the presence of a hydrogen bonding and van der Waals interactions between the molecule and the pristine material. In hand, a non-self-consistent dipole correction was required to cancel the presence of any artificial

electrostatic field. The relaxation is applied on the supercell executed with 10^{-3} eV/cell for energy convergence tolerance, a convergence threshold of the maximum forces of 10 eV/Å, 10^{-2} eV/cell for energy SCF threshold, plane-wave basis set energy cut off of 571.0 eV and, under a gamma points K-mesh of 1 x 1 x 1 and OTFG ultrasoft pseudopotential. Second, the final system was calculated using a Single point calculations (SPC) by Quantum Espresso [57]–[59]. The system was calculated where Grimme-D3 and Gaussian smearing were used for van der Waals, a saw-like electric field potential, and ionic dipole corrections. In addition, the wave function and charge density cutoffs were 60Ry and 480Ry, respectively. The energy convergence threshold of 10^{-5} and atomic pseudopotentials were extracted from the Standard solid-state pseudopotentials (SSSP) available on Materials Cloud[89] [90] [91].

SCF and NSCF calculations for electronic properties

The electronic properties are essential to determine if the pristine material can be used as an electrode for the non-enzymatic glucose sensor. Any drastic change in the electronic property of the 2D graphene and borophene can indicate how the sensor will be able to detect β- glucose. The density of states (DOS) is one of the most commonly used techniques to track the electron distribution near the conduction and valence bands. In order to extract it, rigorous single point calculations (SPC), also known as Self-consistent calculations (SCF) must be done. First, the exchange-correlation functional was GGA PBE, a wave function cutoff of 60Ry and charge density cutoff of 480Ry were used to reach an energy convergence threshold of 10^{-3} and k-mesh 4x4x1. A Projected Augmented Wave (PAW) pseudopotentials of the atoms were extracted from the Standard solid-state pseudopotentials (SSSP) available on Materials Cloud [89] [90] [91]. However, the system wasn't able to converge with the SSSP as it required computational resources that was not available. For that reason, we changed the pseudopotential to Garrity, Bennett, Rabe, and Vanderbilt (GBRV) [93], with a cold smearing and a k-mesh of 4x4x1 along with a wave function cutoff of 40Ry and charge density cutoff of 200Ry to reach an energy and force convergence threshold of $2*10^{-3}$ & $1*10^{-4}$ respectively. The same were used in the non-self-consistent calculations (NSCF) but the we changed the occupation to tetrahedral and k-mesh of 8x8x1 for more accuracy.

The reason why the GBRV pseudopotentials converged faster than PAW pseudopotential is due to the way both were constructed. The PAW pseudopotential approach converts all-electron wave functions into plane waves and projectors. Projectors correct the plane wave basis set near atomic nuclei, where the wave function is very variable and electron density is high. In DFT computations, pseudo wave functions describe valence electrons while non-interacting pseudo-core electrons replace core electrons. This DFT-accepted approach is computationally efficient. The GBRV pseudopotentials are created by fitting the all-electron wave functions in the valence electron region. The fitting uses several *ab initio* computations to produce pseudopotentials that are transportable between materials. The GBRV pseudopotentials have been extensively tested and have proven to be suitable for studying a wide range of materials[90], [93]. As for the electronic occupations the cold smearing wasn't used as it provides less accuracy for the electronic state probability distribution at low k-mesh[94], [95]. Tetrahedral method is more accurate as it is relying on determining the state density by interpolating electronic occupations allocations for large lattices and smaller k-mesh size[96], [97].

DFT Relaxation and SPC calculations of the system in the presence of Platinum substrate

Any 2D pristine material should be above a certain substrate to be able to physically handle it[75], [76],[71], [98], [99]. Platinum substrate is one of the most commonly used in glucose sensors[71], [98], [100]. In order to study the influence of the Platinum substrate, first Pt<111> is added to the graphene lattice, but in case of borophene, Pt<100> is introduced to its lattice since the borophene lattice is a cuboid. In order to relax the supercell, relaxation model available in Quantum Espresso was used[80]–[82]. The *ab-initio* calculations were conducted within the exchange correlation functional of GGA PBEsol. The system was calculated with charge density cutoff of 480Ry and a wave function cutoff of 60Ry. Since platinum is metallic the magnetization model has been also introduced with a polarized spin in z axis calculations Moreover, a fermi-dirac smearing was used along with Grimme-D3 for van der Waals, a saw-like electric field potential and ionic dipole corrections to overcome the underestimation of the dispersion interactions due to the presence of a noncovalent bonding. An energy convergence threshold of 10^{-4} eV and a k-mesh of 1x1x1. The pseudopotentials of the atoms were extracted from the Standard solid-state pseudopotentials (SSSP) available on Materials Cloud [89] [90] [91].

Chapter 4

Results & Discussion

Validity of the Adsorption locator

Since the adsorption locator rely on semi empirical kinetic energy Monte Carlo simulations for time reduction, a relaxation calculation using DFT were required to prove the efficiency and accuracy of these calculations. The relaxation calculations using Quantum Espresso (QE) [80]–[82] as stated above. However, since the two methods have different datum, their energies can't be compared. So for comparison the distances and orientation of the adsorbate molecule is utilized. As shown in the top view in Figure 8, orientation of the glucose didn't differ much between the Adsorption Locator and QE in case of graphene the distances from the pristine graphene and center axis of the glucose molecule was only 4.339 and 4.356 Å. Also the minimum distance differed only by 0.015Å with an error below the 1%.

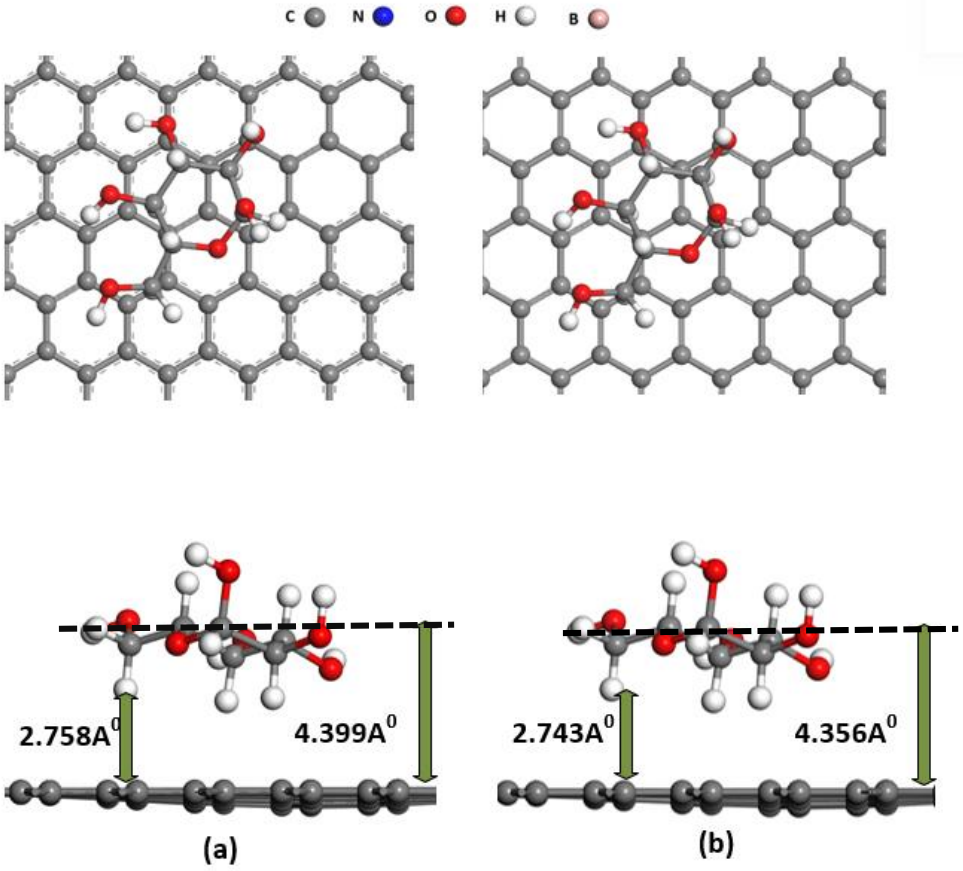

Figure 8: The top and front view of glucose's orientation and distance on graphene output from (a) Adsorption Locator (b) Quantum Espresso relaxation

The same output can be spotted also in the interaction between glucose and borophene in Figure 9. The orientation of the molecule remained the same. However, the distance from the center of the borophene structure to the center axis for the glucose molecule differed from 4.339 Å to 4.356 Å by using Adsorption Locator and QE respectively. The minimum distance changed from 2.758 Å to 2.743 Å where the recorded error is less than 1%. This indicates that the adsorption locator has successfully predicted the orientation and the position of the adsorbate within a matter of minutes while the QE can also reach the same orientation within hours. This gives the advantage for adsorption locator since it provides an acceptable accuracy with great reduction in the computational time and power.

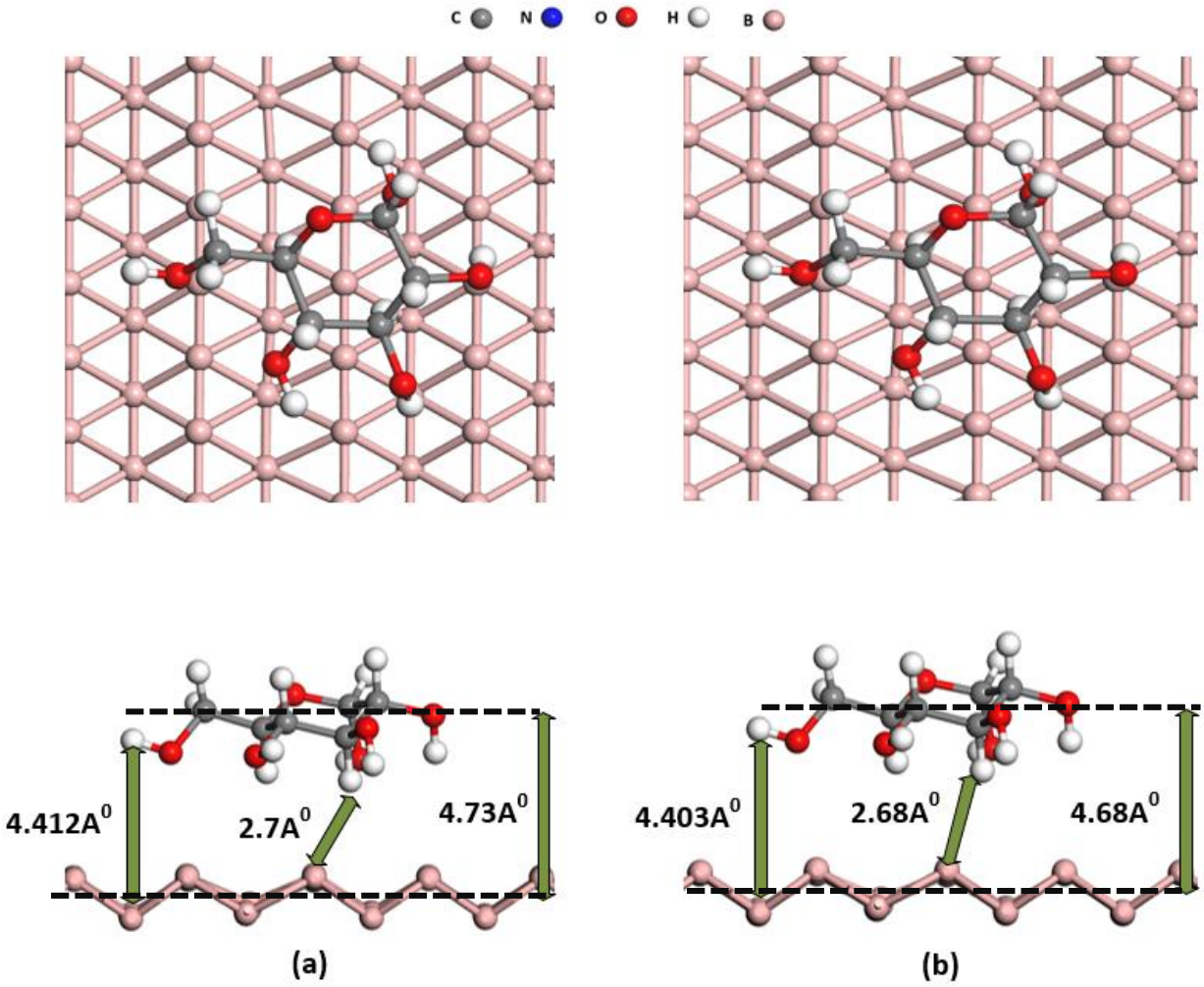

Figure 9: The top and front view of glucose's orientation and distance on borophene output from (a) Adsorption Locator (b) Quantum Espresso relaxation

Binding Energies and Adsorption

The Binding energies have been calculated for each molecule on both the graphene and borophene substrates as follows:

$$E_{binding} = E_{total} - E_{analyte} - E_{pristine}$$

For the molecules studied, Borophene demonstrated notably higher binding energies compared to Graphene. Specifically, Borophene exhibited the highest affinity for uric acid, acetaminophen, and ascorbic acid with binding energies of -4.85 eV, -3.35 eV, and -3.27 eV respectively. Meanwhile, glucose and fructose displayed lower binding energies of -1.16 eV and -1.03 eV respectively. On the other hand, the highest binding energies on the Graphene substrate were for acetaminophen, ascorbic acid, and glucose, measured at -0.74 eV, -0.70 eV, and -0.54 eV respectively, while the binding energy for uric acid was significantly lower at 0.02 eV.

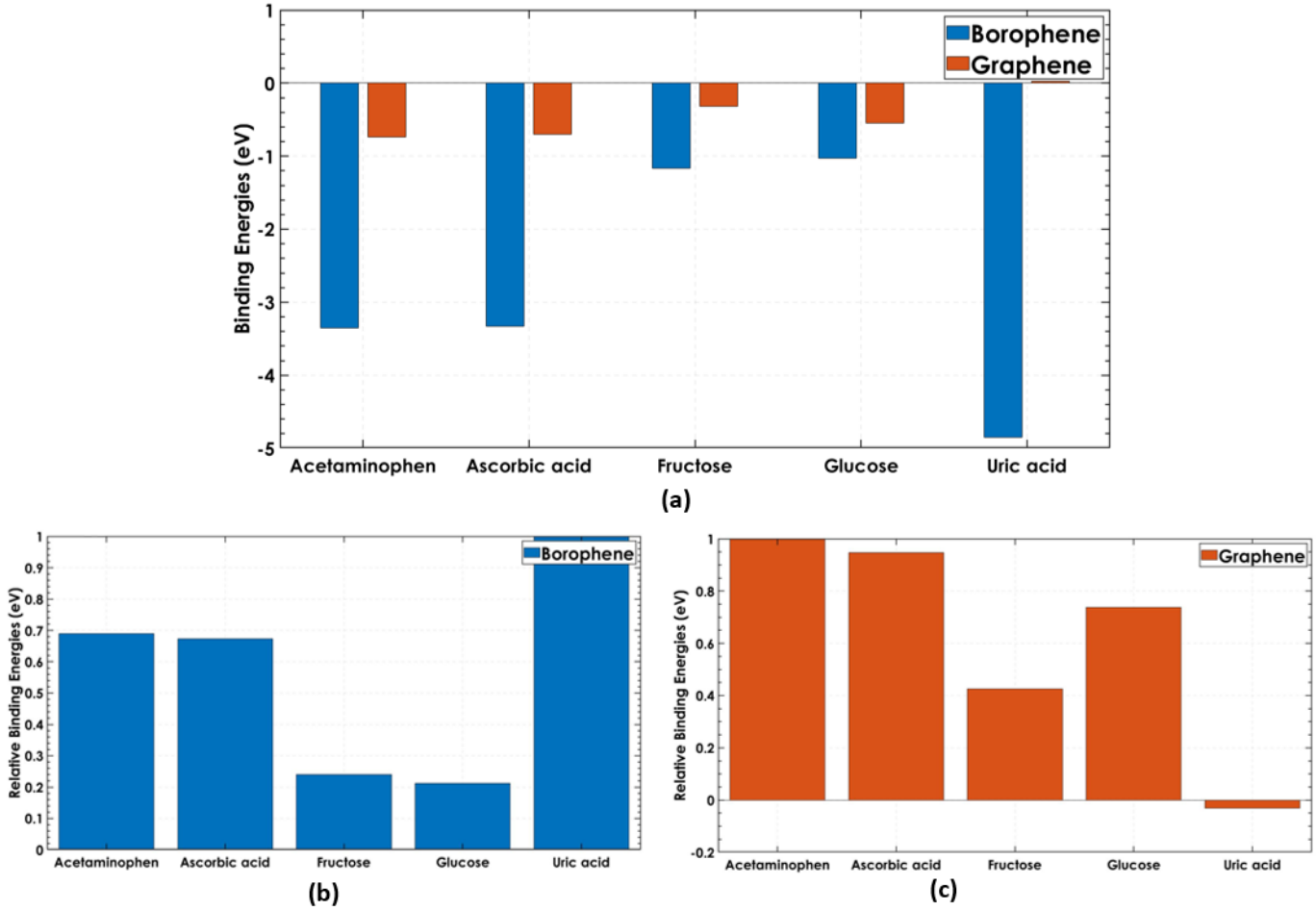

Figure 10: (a)A comparison between the binding energies of organic molecules on Borophene and Graphene substrate (b) relative binding energies of adsorbates on borophene substrate to uric acid (c) relative binding energies of adsorbates on graphene substrate to Acetaminophen

Given the findings of L.Guo et al.[101], suggesting that a material can serve as a suitable sensor if its binding energy exceeds -0.5 eV, both Borophene and Graphene might function as sensors for these compounds. Despite the relatively lower binding energies for glucose on Borophene (-1.16 eV) and Graphene (-0.54 eV), these values exceed the threshold suggested by Guo et al. [101]Therefore, both materials could potentially serve as non-enzymatic glucose sensors.

Table 2: The Binding energies, minimum distance and Closest group of the adsorbate on the graphene (G) and borophene (B) pristine

	β-glucose		Fructose		Acetaminophen		Ascorbic acid		Uric acid	
Pristine	G	B	G	B	G	B	G	B	G	B
Binding energy (eV)	-0.5442	-1.03	-0.31498	-1.164	-0.73818	-3.349	-0.699	-3.269	0.023	-4.853
Minimum distance (Å)	2.743	2.701	2.747	2.763	2.59	2.614	2.724	2.638	2.916	1.584
Relative Binding energy (eV)	0.737	0.2123	0.4267	0.24	1	0.69	0.947	0.673	-0.0313	1
Closest group	OH^-	OH^-	OH^-	OH^-	CH_3^-	CH_3^-	CH_3^-	CH_3^-	OH^-, NH^{-2}	OH^-, C^-

The reported binding distances are depicted in Table 2. Acetaminophen (paracetamol) and ascorbic acid minimum distances are 2.59 Å and 2.724 Å respectively. While β-glucose and fructose are in a close range to the acetaminophen and ascorbic acid, Uric acid is 2.916 Å away from the graphene. In hand, the same effect can also be tracked with Borophene as uric acid, reported only 1.584 Å. In contrast, glucose and fructose have a distance of 2.701 Å and 2.763 Å.

Tran et al. [102] and Rabchinskii et al. [103] have concluded that one of the most influential cause for binding of a molecule on a graphene surface is the presence of hydroxide anion (OH^-) which lead to a strong van der Waals bonding. As shown in Figure 11 and Table 2, the glucose and fructose is the closest to the graphene sheet and in a specific orientation where the oxygen atom is almost above the carbon atom on the graphene sheet and the attached hydrogen atom is oriented towards the center of the graphene hexagonal which can agree with Tran et al. [102], Rabchinskii et al. [103]. On the other hand, the methanide ion CH_3^- in ascorbic acid and acetaminophen were the closest to the Graphene.

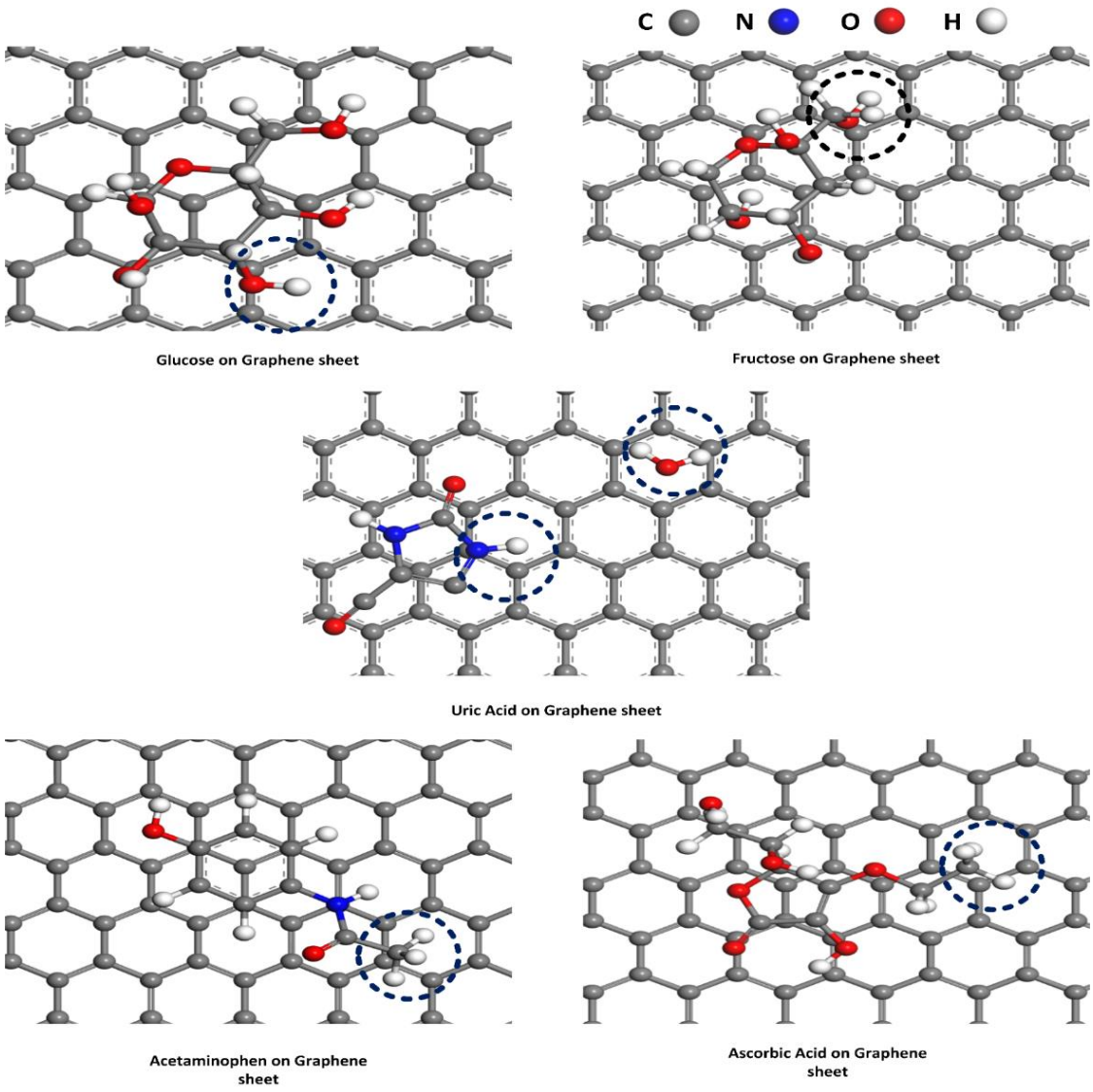

Figure 11: A Top view of the molecules on the pristine 2D graphene and the blue circle highlights the nearest atoms from the pristine material

Furthermore, almost the same ionic groups that are closest to the 2D graphene, are also the same ones that are close to Borophene. As demonstrated in Figure 12, the hydroxide anion in case of β-glucose, fructose and methanide ion for acetaminophen and ascorbic acid. However, the closest group that are attracted on the graphene surface are hydroxide anion OH^- and imidogen NH^{-2} but in case of borophene a partially negative charged C^- and the hydroxide group are attracted to its surface. The C^- led to a drastic

deformation to the 2D borophene as in Figure 12 with a relatively strong binding energy of -4.853 eV and a binding distance of 1.584 Å. It may appear that there is a correlation between the ionic groups and the binding energies on 2D Borophene and Graphene.

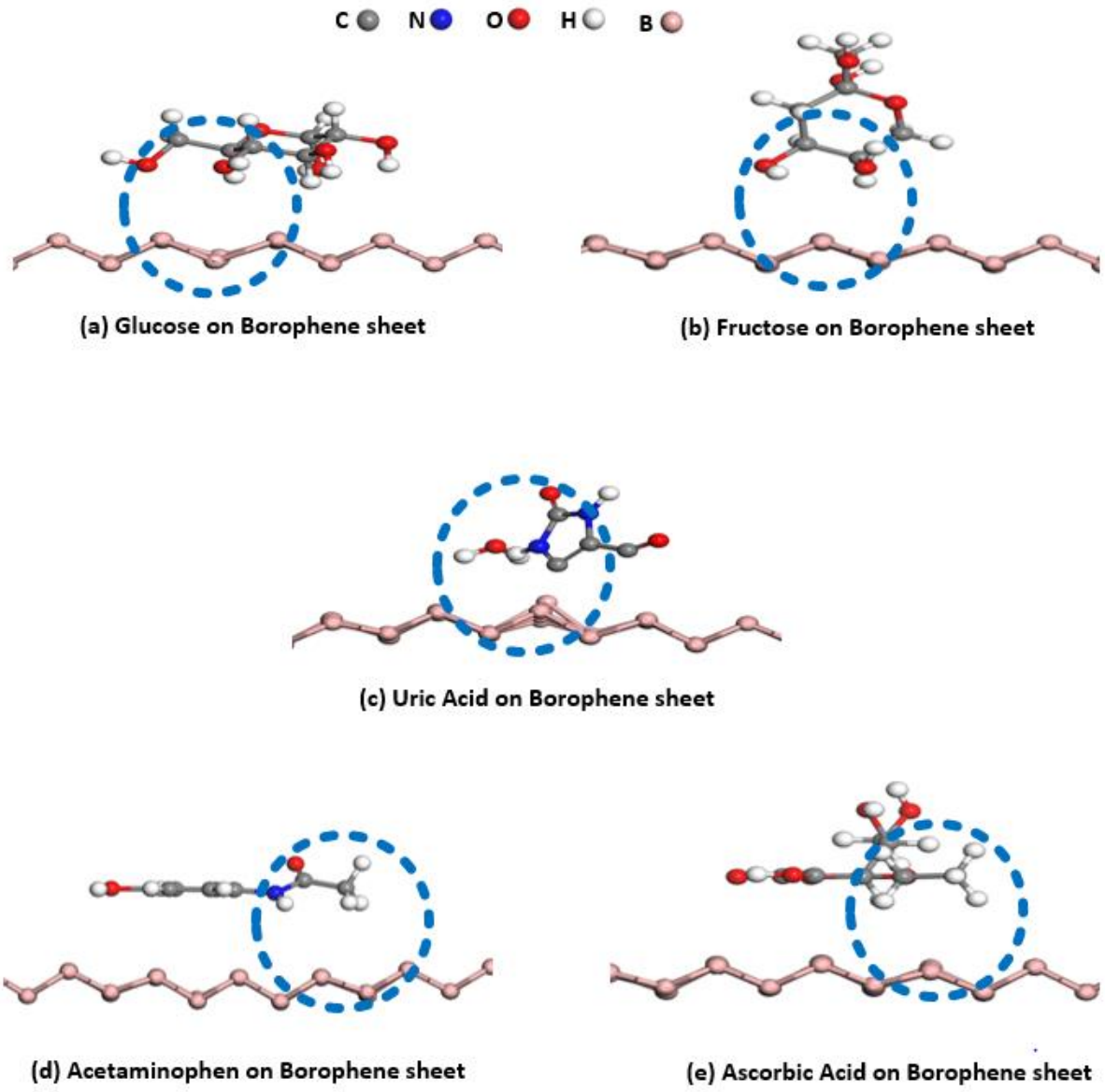

Figure 12: A side view of the molecules on the pristine 2D borophene and the blue circle highlights the nearest atoms from the pristine material

Electronic Structure

In Figure 13, the Density of States (DOS) for both pristine borophene and graphene, as well as with glucose adsorbed on them, is presented. The figures clearly demonstrate that glucose adsorption induces noticeable distortions around the Fermi level in the DOS profiles of both materials. This outcome provides evidence that borophene and graphene, when interacting with glucose, may manifest distinctive electronic responses, thereby hinting at their potential roles as sensors for glucose. However, to confirm this potential, further detailed studies are required. These studies should consider using a higher k-point mesh and energy cut-offs to ensure an even more accurate assessment of the electronic structure alterations in these materials due to glucose interaction. Moreover, transport calculations can be important to confirm how glucose is affecting the electronic conductivity of the graphene based-sensor.

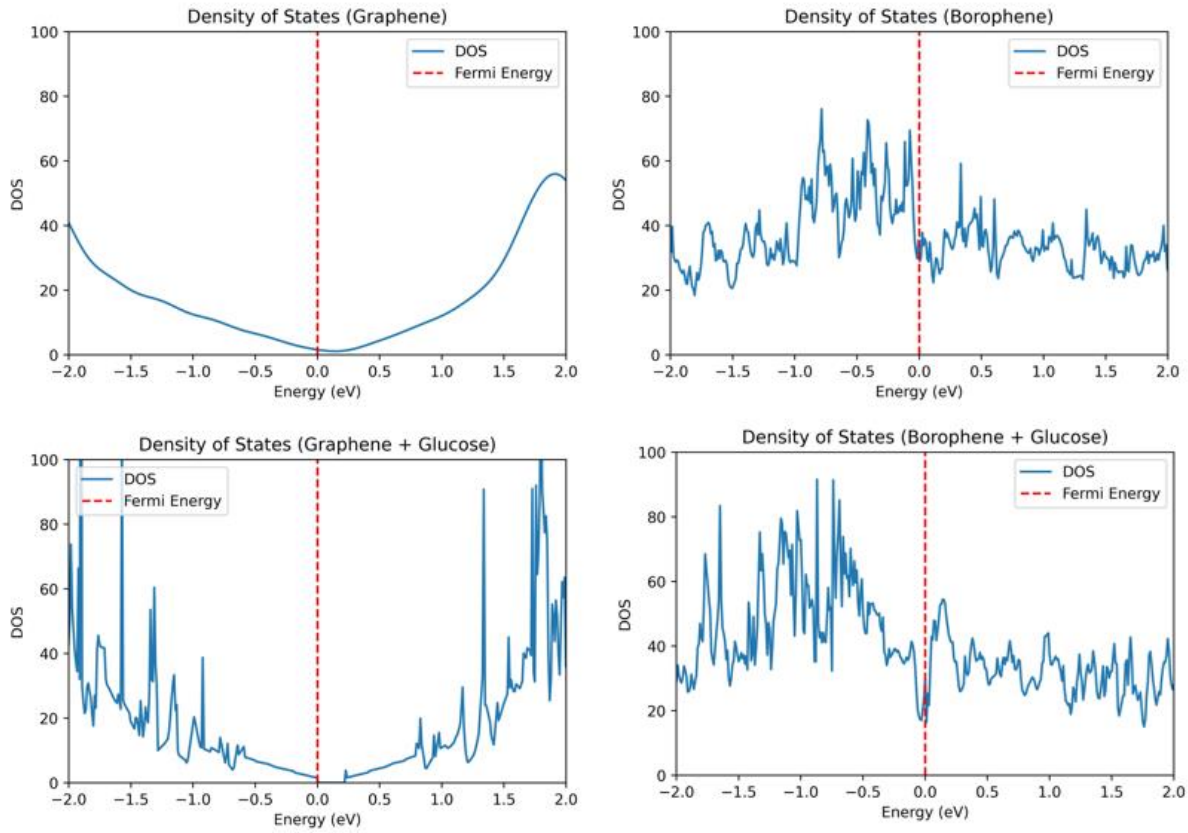

Figure 13: The Density of States of the Pristine materials alone and in the presence of β-glucose where the energy is relative to the Fermi Level

Table 3: The Fermi energy and Dipole moment of the system

	Graphene		Borophene	
	Dipole moment (Ry a.u.)	Delta Dipole moment (Ry a.u.)	Dipole moment(Ry a.u.)	Delta Dipole moment (Ry a.u.)
Pristine alone	-1.0966		-0.0414	
β-Glucose	-1.6418	-0.5452	1.2406	1.282
Fructose	-1.4353	-0.3387	1.244	1.2854
Acetaminophen	-2.044	-0.9474	2.2014	2.2428
Ascorbic acid	-2.0703	-0.9737	2.4714	2.5128
Uric acid	-1.2302	-0.1336	2.7652	2.8066

Effect of Platinum Substrate

The potential influence of substrate materials on the performance of glucose sensors is an area of increasing research interest. Platinum, in particular, due to its excellent electrical conductivity and biocompatibility, has emerged as a promising substrate material. In our study, we observed variations in binding distances when platinum substrates were introduced to both borophene and graphene (as depicted in Figures 15). These preliminary findings highlight the need for further refined calculations and experimental validations to fully comprehend the influence of platinum substrates. For more detailed insights on the interaction of platinum with β-glucose on graphene, please refer to the work of Sakr et al. [71], [98], [100].

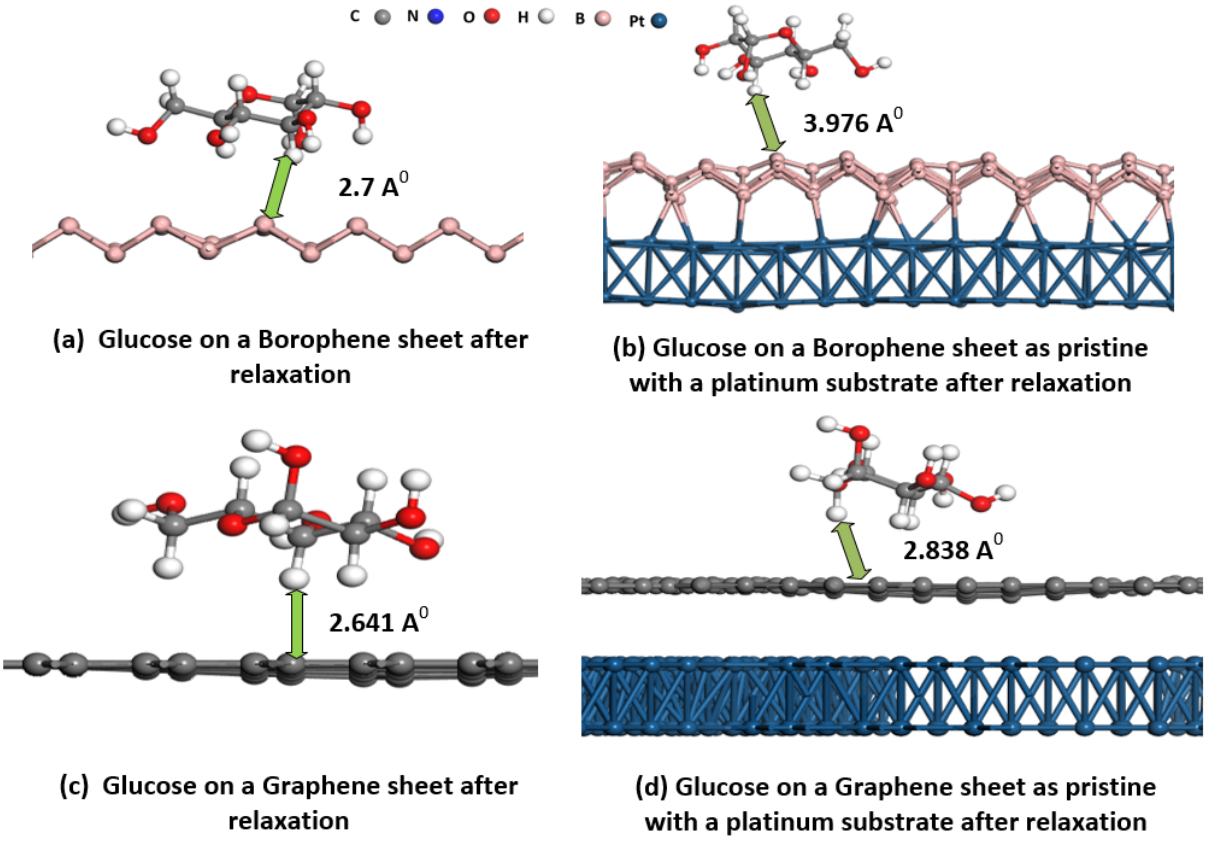

(a) Glucose on a Borophene sheet after relaxation

(b) Glucose on a Borophene sheet as pristine with a platinum substrate after relaxation

(c) Glucose on a Graphene sheet after relaxation

(d) Glucose on a Graphene sheet as pristine with a platinum substrate after relaxation

Figure 14: A comparison between the shortest between the glucose and pristine with and without the presence of platinum substrate

Chapter 5

Conclusion

In this study, we have investigated the potential of graphene and borophene as non-enzymatic glucose sensors. Our results indicate that both 2D materials could serve as glucose sensors, with their binding energies for β-glucose exceeding -0.5 eV, as suggested by Guo et al.[101]. The introduction of a platinum substrate reveals binding behavior consistent with existing literature for both materials. Based on this preliminary research, it can be concluded that graphene and borophene may be promising materials for non-enzymatic glucose sensing. However, further detailed studies and calculations are crucial for more comprehensive conclusions.

References

[1] C. of D. C. and Preventation, “World diabetes day,” 2020.

[2] S. P. Nichols, A. Koh, W. L. Storm, J. H. Shin, and M. H. Schoenfisch, “Biocompatible materials for continuous glucose monitoring devices,” *Chem. Rev.*, vol. 113, no. 4, pp. 2528–2549, 2013.

[3] A. Loke, “Diabetes,” *World Health Organization (WHO)*, 2021. [Online]. Available: https://www.who.int/news-room/fact-sheets/detail/diabetes#:~:text=In 2014%2C 8.5%25 of adults,age of 70) from diabetes.

[4] S. A. White, J. A. Shaw, and D. E. Sutherland, “Pancreas transplantation,” *Lancet*, vol. 373, no. 9677, pp. 1808–1817, 2009.

[5] R. W. G. Gruessner and A. C. Gruessner, “The current state of pancreas transplantation,” *Nat. Rev. Endocrinol.*, vol. 9, no. 9, pp. 555–562, 2013.

[6] M. Park and Y. J. Heo, “Biosensing Technologies for Chronic Diseases,” *Biochip J.*, vol. 15, no. 1, pp. 1–13, 2021.

[7] E. H. Yoo and S. Y. Lee, “Glucose biosensors: An overview of use in clinical practice,” *Sensors*, vol. 10, no. 5, pp. 4558–4576, 2010.

[8] M. Marquitan *et al.*, “Miniaturized Amperometric Glucose Sensors Based on Polymer/ Enzyme Modified Carbon Electrodes in the Sub-Micrometer Scale,” *J. Electrochem. Soc.*, vol. 165, no. 12, pp. G3008–G3014, 2018.

[9] M. H. Hassan, C. Vyas, B. Grieve, and P. Bartolo, “Recent advances in enzymatic and non-enzymatic electrochemical glucose sensing,” *Sensors*, vol. 21, no. 14, 2021.

[10] L. Tang, S. J. Chang, C. J. Chen, and J. T. Liu, “Non-invasive blood glucose monitoring technology: A review,” *Sensors (Switzerland)*, vol. 20, no. 23, pp. 1–32, 2020.

[11] N. S. Oliver, C. Toumazou, A. E. G. Cass, and D. G. Johnston, “Glucose sensors: A review of current and emerging technology,” *Diabet. Med.*, vol. 26, no. 3, pp. 197–210, 2009.

[12] A. E. Kownacka *et al.*, “Clinical Evidence for Use of a Noninvasive Biosensor for Tear Glucose as an Alternative to Painful Finger-Prick for Diabetes Management Utilizing a Biopolymer Coating,” *Biomacromolecules*, vol. 19, no. 11, pp. 4504–4511, 2018.

[13] J. R. Roberts, “Urine Dipstick Testing: Everything You Need to Know,” *Emerg. Med. News*, pp. 24–27, 2007.

[14] K. Tian, M. Prestgard, and A. Tiwari, “A review of recent advances in nonenzymatic glucose sensors,” *Mater. Sci. Eng. C*, vol. 41, no. August, pp. 100–118, 2014.

[15] A. Pfützner, A. Caduff, M. Larbig, T. Schrepfer, and T. Forst, “Impact of posture and fixation technique on impedance spectroscopy used for continuous and noninvasive glucose monitoring,” *Diabetes Technol. Ther.*, vol. 6, no. 4, pp. 435–441, 2004.

[16] J. Kost, S. Mitragotri, R. A. Gabbay, M. Pishko, and R. Langer, “Transdermal monitoring of glucose and other analytes using ultrasound,” *Nat. Med.*, vol. 6, no. 3, pp. 347–350, 2000.

[17] G. Volden, A. K. Thorsrud, L. Bjornson, and E. Jellum, “Biochemical composition of suction blister

fluid determined by high resolution multicomponent analysis (capillary gas chromatography-mass spectrometry and two-dimensional electrophoresis)," *J. Invest. Dermatol.*, vol. 75, no. 5, pp. 421–424, 1980.

[18] U. Kiistala, "Suction blister device for separation of viable epidermis from dermis.," *J. Invest. Dermatol.*, vol. 50, no. 2, pp. 129–137, 1968.

[19] G. Rao, P. Glikfeld, and R. H. Guy, "Reverse Iontophoresis: Development of a Noninvasive Approach for Glucose Monitoring," *Pharmaceutical Research: An Official Journal of the American Association of Pharmaceutical Scientists*, vol. 10, no. 12. pp. 1751–1755, 1993.

[20] M. Shehab, S. Ebrahim, and M. Soliman, "Graphene quantum dots prepared from glucose as optical sensor for glucose," *J. Lumin.*, vol. 184, pp. 110–116, 2017.

[21] V. P. Rachim and W. Y. Chung, "Wearable-band type visible-near infrared optical biosensor for non-invasive blood glucose monitoring," *Sensors Actuators, B Chem.*, vol. 286, no. October 2018, pp. 173–180, 2019.

[22] I. L. Jernelv, K. Milenko, S. S. Fuglerud, D. R. Hjelme, R. Ellingsen, and A. Aksnes, "A review of optical methods for continuous glucose monitoring," *Appl. Spectrosc. Rev.*, vol. 54, no. 7, pp. 543–572, 2019.

[23] J. Ju *et al.*, "Surface Enhanced Raman Spectroscopy Based Biosensor with a Microneedle Array for Minimally Invasive in Vivo Glucose Measurements," *ACS Sensors*, vol. 5, no. 6, pp. 1777–1785, 2020.

[24] Z. Vafapour, "Polarization-Independent Perfect Optical Metamaterial Absorber as a Glucose Sensor in Food Industry Applications," *IEEE Trans. Nanobioscience*, vol. 18, no. 4, pp. 622–627, 2019.

[25] L. R. Bornhoeft, A. Biswas, and M. J. McShane, "Composite hydrogels with engineered microdomains for optical glucose sensing at low oxygen conditions," *Biosensors*, vol. 7, no. 1, 2017.

[26] A. S. M. Z. Kausar, A. W. Reza, T. A. Latef, M. H. Ullah, and M. E. Karim, "Optical nano antennas: State of the art, scope and challenges as a biosensor along with human exposure to nano-toxicology," *Sensors (Switzerland)*, vol. 15, no. 4, pp. 8787–8831, 2015.

[27] M. E. Bosch, A. J. R. Sánchez, F. S. Rojas, and C. B. Ojeda, "Recent development in optical fiber biosensors," *Sensors*, vol. 7, no. 6, pp. 797–859, 2007.

[28] M. M. Rahman, A. J. S. Ahammad, J. H. Jin, S. J. Ahn, and J. J. Lee, "A comprehensive review of glucose biosensors based on nanostructured metal-oxides," *Sensors*, vol. 10, no. 5, pp. 4855–4886, 2010.

[29] L. C. Clark and C. Lyons, "Electrode Systems for Continuous Monitoring in Cardiovascular Surgery," *Ann. N. Y. Acad. Sci.*, vol. 102, no. 1, pp. 29–45, 1962.

[30] Frey JW and C. M, "© 1967 Nature Publishing Group," *Nat. Publ. Gr.*, vol. 216, pp. 615–616, 1967.

[31] C. Chen *et al.*, "Recent advances in electrochemical glucose biosensors: A review," *RSC Adv.*, vol. 3, no. 14, pp. 4473–4491, 2013.

[32] Y. Zhang, Y. Hu, G. S. Wilson, D. Moatti-Sirat, V. Poitout, and G. Reach, “Elimination of the Acetaminophen Interference in an Implantable Glucose Sensor,” *Anal. Chem.*, vol. 66, no. 7, pp. 1183–1188, 1994.

[33] C. Malitesta, F. Palmisano, L. Torsi, and P. G. Zambonin, “Glucose Fast-Response Amperometric Sensor Based on Glucose Oxidase Immobilized in an Electropolymerized Poly(o-phenylenediamine) Film,” *Anal. Chem.*, vol. 62, no. 24, pp. 2735–2740, 1990.

[34] S. V. Sasso, R. J. Pierce, R. Walla, and A. M. Yacynych, “Electropolymerized 1, 2-Diaminobenzene as a Means To Prevent Interferences and Fouling and To Stabilize Immobilized Enzyme in Electrochemical Biosensors,” *Anal. Chem.*, vol. 62, no. 11, pp. 1111–1117, 1990.

[35] A. K. M. Kafi, S. Alim, R. Jose, and M. M. Yusoff, “Fabrication of a glucose oxidase/multiporous tin-oxide nanofiber film on Prussian blue–modified gold electrode for biosensing,” *J. Electroanal. Chem.*, vol. 852, no. October, 2019.

[36] R. Alhans, A. Singh, C. Singhal, J. Narang, S. Wadhwa, and A. Mathur, “Comparative analysis of single-walled and multi-walled carbon nanotubes for electrochemical sensing of glucose on gold printed circuit boards,” *Mater. Sci. Eng. C*, vol. 90, no. June 2017, pp. 273–279, 2018.

[37] S. H. Baek *et al.*, “Cu-nanoflower decorated gold nanoparticles-graphene oxide nanofiber as electrochemical biosensor for glucose detection,” *Mater. Sci. Eng. C*, vol. 107, no. August 2019, p. 110273, 2020.

[38] Q. Mei *et al.*, “Electrospinning of highly dispersed Ni/CoO carbon nanofiber and its application in glucose electrochemical sensor,” *J. Electroanal. Chem.*, vol. 847, no. May, 2019.

[39] N. Suzuki *et al.*, “Engineered glucose oxidase capable of quasi-direct electron transfer after a quick-and-easy modification with a mediator,” *Int. J. Mol. Sci.*, vol. 21, no. 3, pp. 1–10, 2020.

[40] F. Boussema *et al.*, “Dawson-type polyoxometalate nanoclusters confined in a carbon nanotube matrix as efficient redox mediators for enzymatic glucose biofuel cell anodes and glucose biosensors,” *Biosens. Bioelectron.*, vol. 109, pp. 20–26, 2018.

[41] J. Lee, K. Hyun, and Y. Kwon, “A study on the stability and sensitivity of mediator-based enzymatic glucose sensor measured by catalyst consisting of multilayer stacked via layer-by-layer,” *J. Ind. Eng. Chem.*, vol. 93, pp. 383–387, 2021.

[42] P. A. Gallay, M. D. Rubianes, F. A. Gutierrez, and G. A. Rivas, “Avidin and Glucose Oxidase-non-covalently Functionalized Multi-walled Carbon Nanotubes: A New Analytical Tool for Building a Bienzymatic Glucose Biosensor,” *Electroanalysis*, vol. 31, no. 10, pp. 1888–1894, 2019.

[43] I. Willner *et al.*, “Electrical wiring of glucose oxidase by reconstitution of FAD-modified monolayers assembled onto Au-electrodes,” *J. Am. Chem. Soc.*, vol. 118, no. 42, pp. 10321–10322, 1996.

[44] M. Zayats, B. Willner, and I. Willner, “Design of amperometric biosensors and biofuel cells by the reconstitution of electrically contacted enzyme electrodes,” *Electroanalysis*, vol. 20, no. 6, pp. 583–601, 2008.

[45] M. Şenel, C. Nergiz, M. Dervisevic, and E. Çevik, “Development of Amperometric glucose biosensor based on reconstitution of glucose oxidase on polymeric 3-Aminophenyl Boronic Acid

Monolayer," *Electroanalysis*, vol. 25, no. 5, pp. 1194–1200, 2013.

[46] M. Tasviri, H. A. Rafiee-Pour, H. Ghourchian, and M. R. Gholami, "Amine functionalized TiO2 coated on carbon nanotube as a nanomaterial for direct electrochemistry of glucose oxidase and glucose biosensing," *J. Mol. Catal. B Enzym.*, vol. 68, no. 2, pp. 206–210, 2011.

[47] D. W. Hwang, S. Lee, M. Seo, and T. D. Chung, "Recent advances in electrochemical non-enzymatic glucose sensors – A review," *Anal. Chim. Acta*, vol. 1033, pp. 1–34, 2018.

[48] P. Rafighi, M. Tavahodi, and B. Haghighi, "Fabrication of a third-generation glucose biosensor using graphene-polyethyleneimine-gold nanoparticles hybrid," *Sensors Actuators, B Chem.*, vol. 232, pp. 454–461, 2016.

[49] P. Bollella and L. Gorton, "Enzyme based amperometric biosensors," *Curr. Opin. Electrochem.*, vol. 10, pp. 157–173, 2018.

[50] N. Gupta, V. Renugopalakrishnan, D. Liepmann, R. Paulmurugan, and B. D. Malhotra, "Cell-based biosensors: Recent trends, challenges and future perspectives," *Biosens. Bioelectron.*, vol. 141, no. April, p. 111435, 2019.

[51] Z. Zhu, L. Garcia-Gancedo, A. J. Flewitt, H. Xie, F. Moussy, and W. I. Milne, "A critical review of Glucose biosensors based on Carbon nanomaterials: Carbon nanotubes and graphene," *Sensors (Switzerland)*, vol. 12, no. 5, pp. 5996–6022, 2012.

[52] A. Weremfo, S. T. C. Fong, A. Khan, D. B. Hibbert, and C. Zhao, "Electrochemically roughened nanoporous platinum electrodes for non-enzymatic glucose sensors," *Electrochim. Acta*, vol. 231, pp. 20–26, 2017.

[53] S. Lee, J. Lee, S. Park, H. Boo, H. C. Kim, and T. D. Chung, "Disposable non-enzymatic blood glucose sensing strip based on nanoporous platinum particles," *Appl. Mater. Today*, vol. 10, pp. 24–29, 2018.

[54] E. Skou, "The electrochemical oxidation of glucose on platinum-I. The oxidation in 1 M H2SO4," *Electrochim. Acta*, vol. 22, no. 4, pp. 313–318, 1977.

[55] L. D. Burke, "Premonolayer oxidation and its role in electrocatalysis," *Electrochim. Acta*, vol. 39, no. 11–12, pp. 1841–1848, 1994.

[56] Y. Hu, X. Niu, H. Zhao, J. Tang, and M. Lan, "Enzyme-free amperometric detection of glucose on platinum-replaced porous copper frameworks," *Electrochim. Acta*, vol. 165, pp. 383–389, 2015.

[57] J. M. Marioli and T. Kuwana, "Electrochemical characterization of carbohydrate oxidation at copper electrodes," *Electrochim. Acta*, vol. 37, no. 7, pp. 1187–1197, 1992.

[58] K. Kano, M. Torimura, Y. Esaka, M. Goto, and T. Ueda, "Electrocatalytic oxidation of carbohydrates at copper(II) -modified electrodes and its application to flow-through detection," *J. Electroanal. Chem.*, vol. 372, no. 1–2, pp. 137–143, 1994.

[59] S. Berchmans, H. Gomathi, and G. P. Rao, "Electrooxidation of alcohols and sugars catalysed on a nickel oxide modified glassy carbon electrode," *J. Electroanal. Chem.*, vol. 394, no. 1–2, pp. 267–270, 1995.

[60] M. Fleischmann, K. Korinek, and D. Pletcher, "The oxidation of organic compounds at a nickel

anode in alkaline solution," *J. Electroanal. Chem.*, vol. 31, no. 1, pp. 39–49, 1971.

[61] Y. Xue *et al.*, "Nanoporous gold chemically de-alloyed from Au-based amorphous thin film for electrochemical nonenzymatic H2O2 sensing," *Chem. Phys. Lett.*, vol. 723, no. February, pp. 22–27, 2019.

[62] L. Han, S. Zhang, L. Han, D. P. Yang, C. Hou, and A. Liu, "Porous gold cluster film prepared from Au@BSA microspheres for electrochemical nonenzymatic glucose sensor," *Electrochim. Acta*, vol. 138, pp. 109–114, 2014.

[63] N. Verma, "A green synthetic approach for size tunable nanoporous gold nanoparticles and its glucose sensing application," *Appl. Surf. Sci.*, vol. 462, no. August, pp. 753–759, 2018.

[64] J. Li, P. Koinkar, Y. Fuchiwaki, and M. Yasuzawa, "A fine pointed glucose oxidase immobilized electrode for low-invasive amperometric glucose monitoring," *Biosens. Bioelectron.*, vol. 86, pp. 90–94, 2016.

[65] F. Xiao, F. Zhao, D. Mei, Z. Mo, and B. Zeng, "Nonenzymatic glucose sensor based on ultrasonic-electrodeposition of bimetallic PtM (M = Ru, Pd and Au) nanoparticles on carbon nanotubes-ionic liquid composite film," *Biosens. Bioelectron.*, vol. 24, no. 12, pp. 3481–3486, 2009.

[66] S. Ben Aoun, Z. Dursun, T. Koga, G. S. Bang, T. Sotomura, and I. Taniguchi, "Effect of metal ad-layers on Au(1 1 1) electrodes on electrocatalytic oxidation of glucose in an alkaline solution," *J. Electroanal. Chem.*, vol. 567, no. 2, pp. 175–183, 2004.

[67] J. Wang, D. Zhao, and C. Xu, "Nonenzymatic electrochemical sensor for glucose based on nanoporous platinum-gold alloy," *J. Nanosci. Nanotechnol.*, vol. 16, no. 7, pp. 7145–7150, 2016.

[68] K. C. Lin, C. Y. Yang, and S. M. Chen, "Fabrication of a nonenzymatic glucose sensor based on multi-walled carbon nanotubes decorated with platinum and silver hybrid composite," *Int. J. Electrochem. Sci.*, vol. 10, no. 5, pp. 3726–3737, 2014.

[69] S. N. A. Mohd Yazid, I. Md Isa, S. Abu Bakar, N. Hashim, and S. Ab Ghani, "A Review of Glucose Biosensors Based on Graphene/Metal Oxide Nanomaterials," *Anal. Lett.*, vol. 47, no. 11, pp. 1821–1834, 2014.

[70] A. Caglar, D. Düzenli, I. Onal, I. Tezsevin, O. Sahin, and H. Kivrak, "A comparative experimental and density functional study of glucose adsorption and electrooxidation on the Au-graphene and Pt-graphene electrodes," *Int. J. Hydrogen Energy*, vol. 45, no. 1, pp. 490–500, 2020.

[71] M. A. Sakr, K. Elgammal, A. Delin, and M. Serry, "Sensor Based on Graphene-Heterostructure," *PMC Journals*, vol. 20(1), pp. 1–15, 2020.

[72] P. Panigrahi *et al.*, "Two-dimensional Nitrogenated Holey Graphene (C2N) monolayer based glucose sensor for diabetes mellitus," *Appl. Surf. Sci.*, vol. 573, no. October 2021, p. 151579, 2022.

[73] D. Düzenli, I. Onal, and I. Tezsevin, "Investigation of glucose electrooxidation mechanism over N-modified metal-doped graphene," *J. Comput. Chem.*, 2022.

[74] Z. Xie *et al.*, "Two-Dimensional Borophene: Properties, Fabrication, and Promising Applications," *Research*, vol. 2020, pp. 1–23, 2020.

[75] C. Taşaltın, “Glucose sensing performance of PAN: β-rhombohedral borophene based non-enzymatic electrochemical biosensor,” *Inorg. Chem. Commun.*, vol. 133, no. June, 2021.

[76] C. Taşaltın, T. A. Türkmen, N. Taşaltın, and S. Karakuş, “Highly sensitive non-enzymatic electrochemical glucose biosensor based on PANI: β12 Borophene,” *Journal of Materials Science: Materials in Electronics*, vol. 32, no. 8. pp. 10750–10760, 2021.

[77] S. Grimme, C. Bannwarth, and P. Shushkov, “A Robust and Accurate Tight-Binding Quantum Chemical Method for Structures, Vibrational Frequencies, and Noncovalent Interactions of Large Molecular Systems Parametrized for All spd-Block Elements (Z = 1-86),” *J. Chem. Theory Comput.*, vol. 13, no. 5, pp. 1989–2009, 2017.

[78] C. Bannwarth *et al.*, “Extended tight-binding quantum chemistry methods.pdf,” *WIRES Comput. Mol. Sci.*, 2020.

[79] R. L. C. Akkermans, N. A. Spenley, and S. H. Robertson, “Monte carlo methods in materials studio,” *Molecular Simulation*, vol. 39, no. 14–15. Taylor & Francis, pp. 1153–1164, 2013.

[80] P. Giannozzi *et al.*, “Quantum ESPRESSO toward the exascale,” *J. Chem. Phys.*, vol. 152, no. 15, 2020.

[81] P. Giannozzi *et al.*, “QUANTUM ESPRESSO: A modular and open-source software project for quantum simulations of materials,” *J. Phys. Condens. Matter*, vol. 21, no. 39, 2009.

[82] P. Giannozzi *et al.*, “Advanced capabilities for materials modelling with Quantum ESPRESSO,” *J. Phys. Condens. Matter*, vol. 29, no. 46, 2017.

[83] Y. P. Zhou and J. W. Jiang, “Molecular dynamics simulations for mechanical properties of borophene: Parameterization of valence force field model and Stillinger-Weber potential,” *Sci. Rep.*, vol. 7, no. October 2016, pp. 1–12, 2017.

[84] H. Wang, Q. Li, Y. Gao, F. Miao, and X. Zhou, “Strain effects on borophene : ideal strength , negative Possion ’ s ratio and phonon instability,” pp. 1–17, 2015.

[85] BIOVIA Daussault Systeme, “Materials Studio, 2017.” San Diego: Dassult Systemes, 2016.

[86] D. M. Maahs *et al.*, “Effect of acetaminophen on CGM glucose in an outpatient setting,” *Diabetes Care*, vol. 38, no. 10, pp. e158–e159, 2015.

[87] Z. Pu, R. Wang, J. Wu, H. Yu, K. Xu, and D. Li, “A flexible electrochemical glucose sensor with composite nanostructured surface of the working electrode,” *Sensors Actuators, B Chem.*, vol. 230, pp. 801–809, 2016.

[88] C. Bannwarth, S. Ehlert, and S. Grimme, “GFN2-xTB - An Accurate and Broadly Parametrized Self-Consistent Tight-Binding Quantum Chemical Method with Multipole Electrostatics and Density-Dependent Dispersion Contributions,” *J. Chem. Theory Comput.*, vol. 15, no. 3, pp. 1652–1671, 2019.

[89] G. Prandini, A. Marrazzo, I. E. Castelli, N. Mounet, and N. Marzari, “Precision and efficiency in solid-state pseudopotential calculations,” *npj Comput. Mater.*, vol. 4, no. 1, 2018.

[90] K. F. Garrity, J. W. Bennett, K. M. Rabe, and D. Vanderbilt, “Pseudopotentials for high-throughput DFT calculations,” *Comput. Mater. Sci.*, vol. 81, pp. 446–452, 2014.

[91] K. Lejaeghere *et al.*, “Reproducibility in density functional theory calculations of solids,” *Science (80-.).*, vol. 351, no. 6280, 2016.

[92] S. J. Clark *et al.*, “First principles methods using CASTEP,” *Zeitschrift fur Krist.*, vol. 220, no. 5–6, pp. 567–570, 2005.

[93] K. F. Garrity, “GBRV update and JTH testing,” vol. 20899, pp. 1–9, 2014.

[94] F. J. dos Santos and N. Marzari, “Fermi energy determination for advanced smearing techniques,” pp. 1–10, 2022.

[95] M. Methfessel and A. T. Paxton, “High-precision sampling for Brillouin-zone integration in metals,” *Phys. Rev. B*, vol. 40, no. 6, pp. 3616–3621, 1989.

[96] M. Kawamura, Y. Gohda, and S. Tsuneyuki, “Improved tetrahedron method for the Brillouin-zone integration applicable to response functions,” *Phys. Rev. B - Condens. Matter Mater. Phys.*, vol. 89, no. 9, 2014.

[97] C. L. Fu and K. M. Ho, “First-principles calculation of the equilibrium ground-state properties of transition metals: Applications to Nb and Mo,” *Phys. Rev. B*, vol. 28, no. 10, pp. 5480–5486, 1983.

[98] M. A. Sakr and M. Serry, “Non-enzymatic graphene-based biosensors for continous glucose monitoring,” *2015 IEEE SENSORS - Proc.*, no. November 2015, 2015.

[99] R. Reghunath, K. devi, and K. K. Singh, “Recent advances in graphene based electrochemical glucose sensor,” *Nano-Structures and Nano-Objects*, vol. 26, p. 100750, 2021.

[100] M. Serry and M. A. Sakr, “Graphene-metal-semiconductor composite structure for multimodal energy conversion,” *Sensors Actuators, A Phys.*, vol. 245, pp. 169–179, 2016.

[101] L. Guo *et al.*, “Improved NO2 Gas Sensing Properties of Graphene Oxide Reduced by Two-beam-laser Interference,” *Sci. Rep.*, vol. 8, no. 1, pp. 1–7, 2018.

[102] T. T. Tran, T. C. Vu, H. Van Hoang, W. F. Huang, H. T. Pham, and H. M. T. Nguyen, “How are Hydroxyl Groups Localized on a Graphene Sheet?,” *ACS Omega*, vol. 7, no. 42, pp. 37221–37228, 2022.

[103] M. K. Rabchinskii *et al.*, “Manifesting Epoxide and Hydroxyl Groups in XPS Spectra and Valence Band of Graphene Derivatives,” *Nanomaterials*, vol. 13, no. 1, 2023.

Appendices

Adsorption Locator Validation

Appendix A.1 Graphene with Glucose input files

```
&CONTROL
 restart_mode = 'restart'
 calculation = 'relax'
 outdir = './out/'
 prefix = 'gg_ads_loca_valid_BOMD'
 pseudo_dir = './'
 dt = 41.3
 nstep = 100
 tefield = .true.
 dipfield=.true.
 max_seconds = 35000
/
&SYSTEM
 degauss =   0.2
 ecutrho =   4.8000000000d+02
 ecutwfc =   6.0000000000d+01
 ibrav = 0
 nat = 224
 nosym = .false.
 ntyp = 3
 occupations = 'smearing'
 smearing = 'gaussian'
 vdw_corr = 'Grimme-D3'
 emaxpos=0.9
```

```
 eopreg=0.04
 eamp=0
/
&ELECTRONS
 conv_thr =   1.0000000000d-05
 mixing_beta =   0.3
/
&ions
 pot_extrapolation = 'second-order'
 wfc_extrapolation = 'second-order'
 ion_temperature = 'initial'
 tempw = 300
/
ATOMIC_SPECIES
C     12.0107 C.pbe-n-kjpaw_psl.1.0.0.UPF
H     1.00794 H.pbe-rrkjus_psl.1.0.0.UPF
O     15.9994 O.pbe-n-kjpaw_psl.0.1.UPF

ATOMIC_POSITIONS angstrom
O           7.984140000      16.661870000      6.4173800000   1   1   1
C           6.679080000      16.614260000      5.8462200000   1   1   1
C           6.040190000      15.301330000      6.2520100000   1   1   1
O           7.964130000      13.791100000      5.9406400000   1   1   1
H           8.384190000      17.529790000      6.1400900000   1   1   1
…           ……              ……..              ……..           ..   ..   ..
…           ……              ……..              ……..           ..   ..   ..
…           ……              ……..              ……..           ..   ..   ..
C         -12.381470000      21.444990000      2.2140500000   0   0   0
```

C 0.001460000 1.429170000 2.2161000000 0 0 0

C 2.477760000 -0.000210000 2.2075300000 0 0 0

K_POINTS automatic

1 1 1 0 0 0

CELL_PARAMETERS angstrom

24.7640000000 0.0000000000 0.0000000000

-12.3823400000 21.4460600000 0.0000000000

0.0000000000 0.0000000000 18.6227000000

Appendix A.2 Borophene with Glucose input files

```
&CONTROL
  restart_mode = 'restart'
  calculation = 'relax'
  outdir = './out/'
  prefix = 'gb_ads_loca_valid_BOMD'
  pseudo_dir = './'
  dt = 41.3
  nstep = 100
  tefield = .true.
  dipfield=.true.
  max_seconds = 35000
/
&SYSTEM
  degauss =   0.2
  ecutrho =   4.8000000000d+02
  ecutwfc =   6.0000000000d+01
  ibrav = 0
  nat = 224
  nosym = .false.
  ntyp = 4
  occupations = 'smearing'
  smearing = 'gaussian'
  vdw_corr = 'Grimme-D3'
  emaxpos=0.9
  eopreg=0.04
  eamp=0
```

```
/
&ELECTRONS
  conv_thr =   1.0000000000d-05
  mixing_beta =   0.3
/
&ions
  pot_extrapolation = 'second-order'
  wfc_extrapolation = 'second-order'
  ion_temperature = 'initial'
  tempw = 300
/
ATOMIC_SPECIES
B      10.811 b_pbe_v1.4.uspp.F.UPF
C      12.0107 C.pbe-n-kjpaw_psl.1.0.0.UPF
H      1.00794 H.pbe-rrkjus_psl.1.0.0.UPF
O      15.9994 O.pbe-n-kjpaw_psl.0.1.UPF
ATOMIC_POSITIONS angstrom
C           8.130745         11.055702         7.425357     1    1    1
C           7.352877         10.053577         8.274342     1    1    1
O           9.411421          8.713543         8.462931     1    1    1
O           7.781909          8.192614         6.867264     1    1    1
H          13.393716          9.874647         7.345399     1    1    1
H          11.773161          9.996329         9.031793     1    1    1
…           ……           ……           ……..    ..     ..    ..
…           ……           ……           ……..    ..     ..    ..
…           ……           ……           ……..    ..     ..    ..
B           0.492575          6.849156         3.933977     0    0    0
B           1.896637          7.668587         2.996419     0    0    0
```

B 3.301002 6.849647 3.933708 0 0 0

K_POINTS automatic

1 1 1 0 0 0

CELL_PARAMETERS angstrom

28.6428000000 0.0000000000 0.0000000000

0.0456200000 16.3558400000 0.0000000000

0.0000000000 -0.0000500000 13.4610000000

Platinum Effect QE files

Appendix B.1 Graphene with Glucose

```
&CONTROL
 calculation = 'vc-relax'
 restart_mode = 'from_scratch'
 etot_conv_thr =   1.0000000000d-04
 forc_conv_thr =   1.0000000000d-04
 outdir = './out/'
 nstep=  100
 prefix = 'ptgg'
 pseudo_dir = './pseudo/'
 tprnfor = .true.
 tstress = .true.
 verbosity = 'high'
 max_seconds =  36000
/
&SYSTEM
 degauss =   0.02
 ecutrho =   4.8000000000d+02
 ecutwfc =   6.0000000000d+01
 ibrav = 0
 nat = 512
 nosym = .false.
 nspin = 2
```

```
 ntyp = 4
 occupations = 'smearing'
 smearing = 'fd'
 starting_magnetization(1) =   1.0000000000d-01
 starting_magnetization(2) =   1.0000000000d-01
 starting_magnetization(3) =   1.0000000000d-01
 starting_magnetization(4) =   3.1250000000d-01
/
/
&ELECTRONS
 conv_thr =   1.0000000000d-06
 electron_maxstep = 800
 diagonalization = 'cg'
 mixing_beta =   5.0000000000d-01
/
&IONS
/
&CELL
/
ATOMIC_SPECIES
C     12.0107 C.pbe-n-kjpaw_psl.1.0.0.UPF
H     1.00794 H.pbe-rrkjus_psl.1.0.0.UPF
O     15.9994 O.pbe-n-kjpaw_psl.0.1.UPF
Pt    195.084 pt_pbe_v1.4.uspp.F.UPF
ATOMIC_POSITIONS angstrom
O       15.55370      10.67810      10.99890
C       14.40490      11.27990      10.42020
C       13.10180      10.49970      10.79640
```

… …… …… ……..

… …… …… ……..

… …… …… ……..

Pt 5.47560 1.05410 3.80180

Pt 7.30080 0.00010 3.80190

K_POINTS automatic

2 2 2 0 0 0

CELL_PARAMETERS angstrom

25.2912000000 0.0000000000 0.0000000000

-12.6462322820 21.9030339898 0.0000000000

0.0002108820 -0.0000243471 24.1652999991

Appendix B.2 Borophene

```
&CONTROL
  calculation = 'vc-relax'
  restart_mode = 'from_scratch'
  etot_conv_thr =   1.0000000000d-04
  forc_conv_thr =   1.0000000000d-04
  outdir = './out/'
  prefix = 'aiida'
  pseudo_dir = './pseudo/'
  nstep=100
  tprnfor = .true.
  tstress = .true.
  verbosity = 'high'
  max_seconds =  36000
/
&SYSTEM
  degauss =   2.2049585400d-02
  ecutrho =   4.8000000000d+02
  ecutwfc =   6.0000000000d+01
  ibrav = 0
  nat = 352
  nosym = .false.
  nspin = 2
  ntyp = 5
  occupations = 'smearing'
  smearing = 'fd'
```

```
 starting_magnetization(1) =   1.0000000000d-01
 starting_magnetization(2) =   1.0000000000d-01
 starting_magnetization(3) =   1.0000000000d-01
 starting_magnetization(4) =   1.0000000000d-01
 starting_magnetization(5) =   3.1250000000d-01
/
&ELECTRONS
 conv_thr =   1.0000000000d-06
 electron_maxstep = 800
 mixing_beta =   1.0000000000d-01
/
&IONS
/
&CELL
/
ATOMIC_SPECIES
B     10.811 b_pbesol_v1.4.uspp.F.UPF
C     12.0107 C.pbesol-n-kjpaw_psl.1.0.0.UPF
H     1.00794 H.pbesol-rrkjus_psl.1.0.0.UPF
O     15.9994 O.pbesol-n-kjpaw_psl.0.1.UPF
Pt    195.084 pt_pbesol_v1.4.uspp.F.UPF
CELL_PARAMETERS (angstrom)
  28.369626663  -0.037360278  -0.190918050
   0.022902490  16.158563575   0.062078673
  -0.208433104   0.115982907  22.000000000

ATOMIC_POSITIONS (crystal)
B           0.0122802668       0.4149286784       0.3850021052
```

B 0.0627343446 0.4639507929 0.3574418527

B 0.1136124319 0.4147028349 0.3850482977

… …… …… ……..

… …… …… ……..

… …… …… ……..

Pt 0.8750007133 0.7525653296 0.1886976971

Pt 0.8771516604 0.8725979053 0.0481913486

Pt 0.9377683675 0.7471382067 0.0579518235

Pt 0.9388730038 0.8735031658 0.1787028622

K_POINTS automatic

1 1 1 0 0 0

Density of States

Appendix C.1 Graphene SCF

```
&CONTROL
  calculation = 'scf'
  restart_mode = 'from_scratch'
  etot_conv_thr =   2.0000000000d-03
  forc_conv_thr =   1.0000000000d-04
  outdir = './out/'
  prefix = 'aiida'
  pseudo_dir = './'
!  tprnfor = .true.
!  tstress = .true.
  verbosity = 'high'
/
&SYSTEM
  degauss =   2.2049585400d-02
  ecutrho =   200
  ecutwfc =   40
  ibrav = 0
  nat = 200
  nosym = .false.
  ntyp = 1
  occupations = 'smearing'
  smearing = 'cold'
/
&ELECTRONS
  conv_thr =   4.0000000000d-08
```

```
 electron_maxstep = 80
 mixing_beta =   4.0000000000d-01
/
ATOMIC_SPECIES
C     12.0107 c_pbe_v1.2.uspp.F.UPF
ATOMIC_POSITIONS crystal
C          0.4500000000      0.0000000000      0.0833333333
C          0.5166666666      0.0333333333      0.0833333333
C          0.4499999999      0.0999999998      0.0833333333
C          0.5166666666      0.1333333331      0.0833333333
…      ……      ……      ……..
…      ……      ……      ……..
…      ……      ……      ……..
C          1.4166666667      0.8333333334      0.0833333333
C          1.3500000000      0.9000000000      0.0833333333
C          1.4166666666      0.9333333333      0.0833333333
K_POINTS automatic
4 4 1 0 0 0
CELL_PARAMETERS angstrom
    24.6000000000      0.0000000000      0.0000000000
   -12.3000000000     21.3042249331      0.0000000000
     0.0000000000      0.0000000000     12.0000000000
```

Appendix C.2 Graphene NSCF

```
&CONTROL
  calculation = 'nscf'
  etot_conv_thr =   2.0000000000d-03
  forc_conv_thr =   1.0000000000d-04
  outdir = './out/'
  prefix = 'aiida'
  pseudo_dir = './'
! tprnfor = .true.
! tstress = .true.
  verbosity = 'high'
/
&SYSTEM
  degauss =   2.2049585400d-02
  ecutrho =   200
  ecutwfc =   40
  ibrav = 0
  nat = 200
  nosym = .false.
  ntyp = 1
  occupations = 'tetrahedra'
  smearing = 'cold'
  nbnd = 480
/
&ELECTRONS
  conv_thr =   4.0000000000d-08
```

```
  electron_maxstep = 80
  mixing_beta =   4.0000000000d-01
/
ATOMIC_SPECIES
C     12.0107 c_pbe_v1.2.uspp.F.UPF
ATOMIC_POSITIONS crystal
C           0.4500000000      0.0000000000      0.0833333333
C           0.5166666666      0.0333333333      0.0833333333
C           0.4499999999      0.0999999998      0.0833333333
…       ……        ……        ……..
…       ……        ……        ……..
…       ……        ……        ……..
C           1.4166666667      0.8333333334      0.0833333333
C           1.3500000000      0.9000000000      0.0833333333
C           1.4166666666      0.9333333333      0.0833333333
K_POINTS automatic
8 8 1 0 0 0
CELL_PARAMETERS angstrom
    24.6000000000      0.0000000000      0.0000000000
   -12.3000000000     21.3042249331      0.0000000000
     0.0000000000      0.0000000000     12.0000000000
```

CASTEP Calculations

Appendix D.1 Methodology

At the beginning of our work we used CASTEP module in Materials Studio [92] to do our DFT calculations as they are much faster. However, we discovered that we were doing something wrong in the input files and hence an incorrect calculations have been produced. In here we present the methodology we used in CASTEP and the results.

DFT relaxation of the Supercell

In order to relax the supercell, Geometry Optimization available in CASTEP module in Materials studio was used[92]. The *ab-initio* calculations were conducted within the exchange correlation functional of GGA PBE. However, the model needed a further correction to overcome the underestimation of the dispersion interactions due to the presence of a noncovalent bonding, Grimme et al. dispersion correction in DFT-D is used. The lattice relaxation is applied on the supercell with an OTFG ultrasoft pseudopotential and a gamma points k-mesh of 1 x 1 x 1 along with a cut-off energy of the basis set, energy convergence, minimum forces and SCF tolerance of 381 eV, 0.01 eV/cell, 10 eV/A^0 and 10^{-5} eV/cell respectively.

DFT Relaxation and SPC calculations of the system

Once the molecule position and orientation is determined using the Adsorption Locator, a first-principle is preformed to calculate the binding energy of the molecules on the pristine materials on two steps. First, a geometry optimization calculations done using CASTEP module in Materials Studio where the molecules are allowed to move freely while the pristine material is fixed[92]. The exchange-correlation functional was GGA PBE and DFT-D Grimme correction is performed due to the presence of a hydrogen bonding and van der Waals interactions between the molecule and the pristine material. In hand, a non-self-consistent dipole correction was required to cancel the presence of any artificial electrostatic field. The relaxation is applied on the supercell executed with 10-3 eV/cell for energy convergance tolerance, a convergence threshold of the maximum forces of 10 eV/A^0, 10^{-2} eV/cell for energy SCF threshold, plane-wave basis set energy cut off of 381.0 eV and, under a gamma points K-mesh of 1 x 1 x 1 and OTFG ultrasoft pseudopotential. Second, the final system was calculated using a Single point calculations (SPC) also by CASTEP module in Materials Studio with the same exchange-correlation functional, a dipole moment and Van-Der Waals correction [92]. The calculation was further enhanced as the SCF tolerance, energy cut-off and gamma k-mesh were chosen to be 10^{-6}eV/cell, 10 eV and 2 x 2 x 1 respectively.

Appendix D.2 CASTEP Results

Binding & Adsorption energies

The Binding energies have been calculated for each molecule on both the graphene and borophene substrates as follows:

$$E_{binding} = E_{total} - E_{analyte} - E_{substrate}$$

As shown in the Figure 15, The binding energies of the molecules are much higher with graphene substrate compared to borophene for example fructose has a -0.3124eV and -0.0534eV with graphene and borophene respectively. In addition, the borophene has no affinity to ascorbic acid and acetaminophen (paracetamol), but graphene has a high affinity for both reaching -0.2662eV and -0.2642eV respectively. It is also highlighted that graphene has a high affinity for fructose, uric acid and glucose as they have binding energies of -0.3124 eV, -0.3292eV and -0.32413eV. Despite the higher binding energy to glucose, fructose and uric acid compared to borophene, the energies are very close to each other indicating no selectivity for the graphene pristine. On the other hand, borophene has demonstrated to have a selectivity despite the low binding energy. The borophene had the highest binding energy of -0.07775eV for uric acid and lowest for glucose with only -0.026476eV, while fructose had a better binding energy of -0.0534eV on borophene surface.

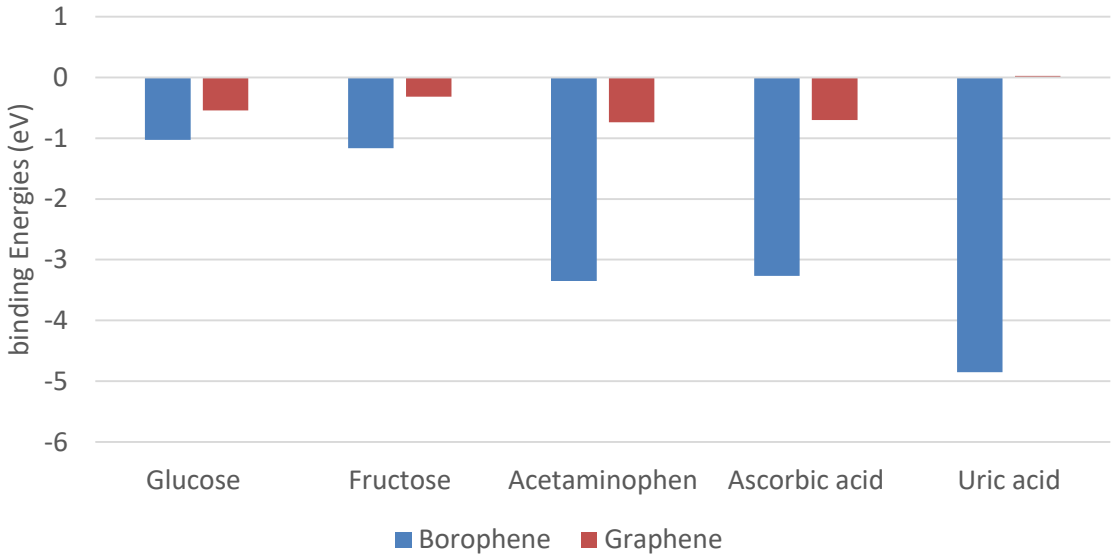

Figure 15: The binding energy of each molecule with graphene and borophene substrate

Density of States

To understand the factors that contribute to the binding energy between the pristine materials and molecules, it's important to investigate the density of states (DOS) and observe any changes that may occur in the electronic properties of the pristine materials. By analyzing the DOS of graphene in Figure 16, there is no significant change in the conduction band. However, a slight shift can be observed in the conduction band in the presence of uric acid, indicating a weak interaction between the graphene and uric acid. However, this shift is not significant enough to cause any major changes in the electronic properties of graphene. This suggests that the strong binding energies observed in Figure 15 between the molecules and graphene are primarily due to van der Waals forces. These forces are known to arise from the interaction between the electron clouds of the two materials, and they can result in strong attractive forces between nonpolar molecules.

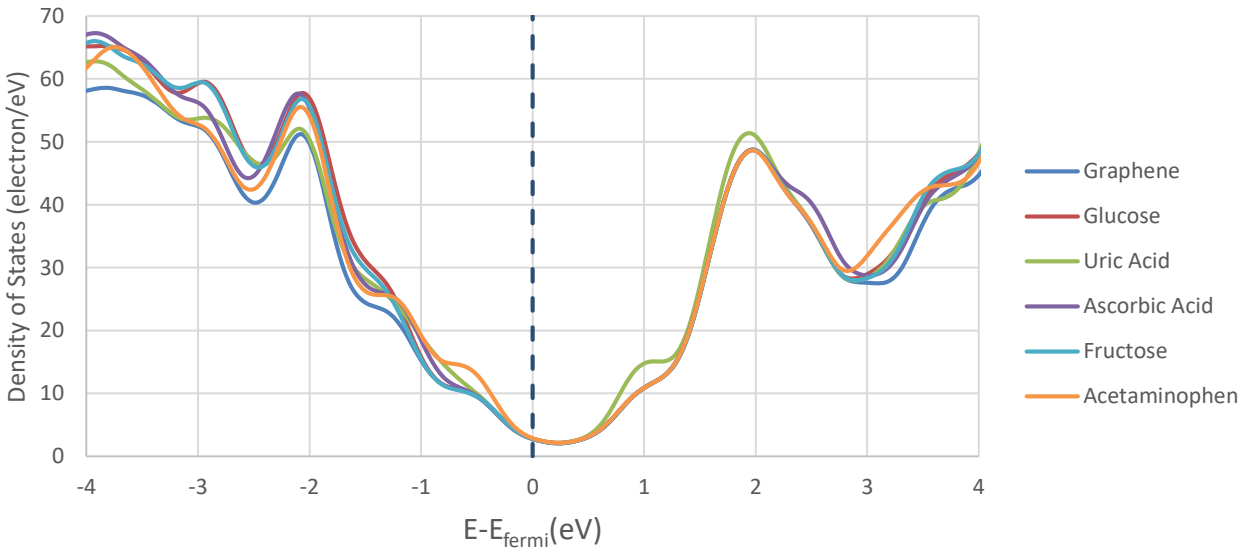

Figure 16: Graphene DOS with different adsorbates and pristine

Another proof of dominance of the van der Waals forces and its influence on the binding energies can be shown in Figure 11. The hydroxide bond that is present in the uric acid, glucose and fructose is the closest to the graphene sheet and in a specific orientation where the oxygen atom is almost above the carbon atom on the graphene sheet and the attached hydrogen atom is oriented towards the center of the graphene hexagonal which agrees with Tran et al.[66], Rabchinskii et al. [67]. In addition, Tran et al. have also highlighted that the hydroxide bonds don't have an effect on the DOS of the graphene [66]. In case of ascorbic acid and acetaminophen in Figure 11, the C-H bond was the one closest to the graphene

sheet and that led to a weaker van der Waals bonding leading to a decrease in the binding energy as illustrated in Figure 15.

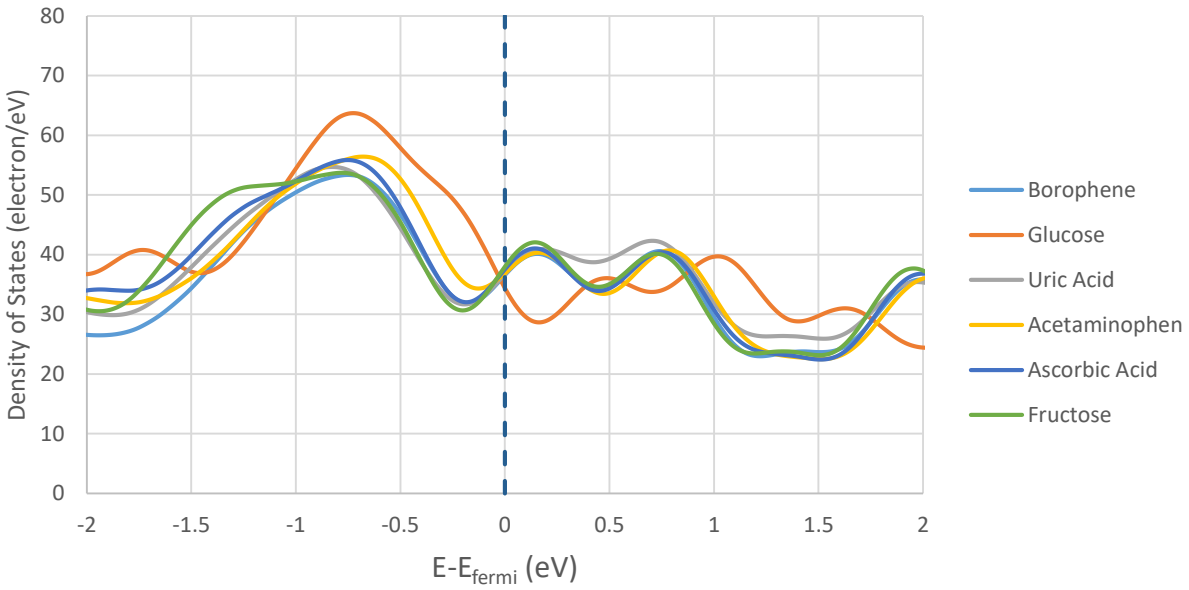

Figure 17: Borophene DOS with different adsorbates and pristine

As shown in **Error! Reference source not found.**, the density of states (DOS), in case of glucose and uric a cid, indicates that the surface of borophene has been modified. This surface functionalization altered the electronic structure of 2D borophene by introducing new energy levels in the valence or conduction bands or by repositioning existing energy levels. As depicted in Figure 15, the resultant changes in the electronic structure and van der Waals forces have led to the formation of strong binding energies between borophene and glucose or uric acid. As shown in **Error! Reference source not found.**, there is n o functionalization of the borophene surface in the cases of ascorbic acid and acetaminophen. As a result, there is no significant change to the borophene's electronic structure, resulting in weaker binding energies between borophene and these molecules.